Composite Structures 271 (2021) 114125

Contents lists available at ScienceDirect

Composite Structures

journal homepage: www.elsevier.com/locate/compstruct

New incremental secant linearization method for mean-field homogenization approach of elasto-viscoplastic microscopic heterogeneous materials

Wei Rao [a,b], Chao Yu [a], Juan Zhang [a], Guozheng Kang [a,*]

[a] Applied Mechanics and Structure Safety Key Laboratory of Sichuan Province, School of Mechanics and Engineering, Southwest Jiaotong University, Chengdu, Sichuan, PR China
[b] State Key Laboratory of Nonlinear Mechanics, Institute of Mechanics, Chinese Academy of Sciences, Beijing 100190, PR China

ARTICLE INFO

Keywords:
Elasto-viscoplastic microscopic heterogeneous materials
Incremental secant linearization method
Mean-field homogenization theory
Micro-mechanics

ABSTRACT

Unmatched time scales of elastic and viscoplastic responses are not reasonably considered in linearizing the constitutive laws of constituent phases in elasto-viscoplastic microscopic heterogeneous materials, which makes the interaction among the constituent phases very difficult to be described by homogenization approaches. To address this issue, a new incremental secant linearization method is developed by solving linearized equations of stress, strain and time increments obtained from the Hooke's law and the Taylor's expansion of stress increment function. Subsequently, the new linearization method is implemented into the Mori-Tanaka's (M − T) and self-consistent (SC) homogenization approaches. Finally, the stress–strain responses of elasto-viscoplastic microscopic heterogeneous materials (including the composites and polycrystalline materials) under different loading conditions are predicted by the incremental secant linearization-based M − T and SC approaches, and the predicted results are compared with the results obtained by other approaches, such as finite element, fast Fourier transform and generalized affine linearization methods. The comparison shows that the new secant linearization takes an important role in the accurate and effective simulations of the stress–-strain responses of elasto-viscoplastic microscopic heterogeneous materials, and the predictions are independent of loading step size if the step size is not too large. Meanwhile, the homogenization approaches of elasto-viscoplastic and elasto-plastic microscopic heterogeneous materials are expected to be unified since the new secant linearization method provides the same mathematical structure for the linearized elasto-viscoplastic constitutive model as that for the elasto-plastic one.

1. Introduction

The effectiveness of mean-field homogenization (MFH) theory in constructing a *meso*-mechanical constitutive model has been widely recognized [1-5]. Thus, the MFH theory has been gotten much attention. In particular, since the Eshelby's inclusion theory was put forward [6], the MFH theory was greatly developed, and a series of representative micromechanics approaches for linear microscopic heterogeneous materials (e.g., composites and polycrystalline aggregates) were proposed, such as the Mori-Tanaka's (M − T) [7], self-consistent (SC) [8-10], second-ordered moment [11], bridging [12], and generalized self-consistent [13] methods. Of course, the validity, capability and efficiency of such MFH approaches in predicting the deformations of the microscopic heterogeneous materials consisting of linear constituents were also proved.

However, the MFH theory of nonlinear (for instances, nonlinear elasticity, plasticity, viscoelasticity and viscoplasticity) microscopic heterogeneous materials becomes more complex. As we know, the Eshelby's inclusion theory regards both matrix and inclusion phases as linearly elastic media. It is no doubt that the above-mentioned MFH approaches of linear heterogeneous materials cannot be directly applied to the heterogeneous materials consisting of nonlinear constituents. Hill [14] thought that the exiting MFH approaches of linear heterogeneous materials could be applied to the nonlinear heterogeneous materials if the nonlinear constitutive model of each constituent could be reasonably linearized. From this point, he firstly applied the SC approach to describe the overall elasto-plastic responses of heterogeneous materials. Subsequently, based on Hill [14], some researchers further extended the MFH approaches to describe the overall responses of nonlinear heterogeneous materials [15-21]. From the Hill's view-

* Corresponding author.
E-mail addresses: guozhengkang@home.swjtu.edu.cn, guozhengkang@126.com (G. Kang).

https://doi.org/10.1016/j.compstruct.2021.114125
Received 20 January 2021; Revised 6 May 2021; Accepted 17 May 2021
Available online 21 May 2021

point [14], the MFH approaches of nonlinear microscopic heterogeneous materials can be established by a procedure containing two steps, i.e., (1) linearize the constitutive law of each constituent; (2) implement the linearized constitutive equations into a MFH scheme. Thus, it could be said that the validity and efficiency of a MFH approach for modeling nonlinear heterogeneous materials depend strongly on the linearization of constituent constitutive models.

For different nonlinear constitutive models, their linearization methods are significantly different from each other. For example, the elasto-plastic constitutive law assumes that such deformations of materials are immediate responses, not dependent on the time. Thus, the stress function is a single-valued function in a small loading step, and the linearization of elasto-plastic constitutive model can be easily conducted based on the idea of differential approximation. An approximate linearized relation between the stress increment $\Delta\boldsymbol{\sigma}$ and strain increment $\Delta\boldsymbol{\varepsilon}$ is simply given, i.e., $\Delta\boldsymbol{\sigma} = \boldsymbol{C}^{\text{alg}} : \Delta\boldsymbol{\varepsilon}$, where $\boldsymbol{C}^{\text{alg}}$ is the algorithmic tangent operator of elasto-plastic constitutive model. With such a linearization method, the overall deformations of elasto-plastic heterogeneous materials were reasonably described by the MFH scheme as shown in Ref. [22]. However, for the elasto-viscoplastic material, its mechanical response is made up of immediate elastic and hysteretic viscoplastic responses, and the responding stress depends on both the applied strain and loading time. Thus, it implies that the linearization methods of elasto-plastic constitutive laws are not suitable for the elasto-viscoplastic ones. At present, several kinds of representative linearization methods have been developed to linearize the elasto-viscoplastic constitutive laws. The linearization forms given by these methods are different from each other. A brief review of linearization methods and corresponding homogenization approaches is conducted as follows:

(1) The approach based on Laplace's transformation [23,24]. Here, the linearized elasto-viscoplastic constitutive law is transformed into the Laplace-Carson's space at first. Since the separation of time scales between elastic deformation and viscoplastic one doesn't exhibit in the Laplace-Carson's space, a fictitious linear thermo-elastic relationship between the stress rate tensor $\dot{\boldsymbol{\sigma}}$ and strain rate tensor $\dot{\boldsymbol{\varepsilon}}$ can be simply given as: $\boldsymbol{\sigma}^*(s) = \boldsymbol{C}^*_\tau(\tau, s) : (\boldsymbol{\varepsilon}^*(s) - \boldsymbol{\varepsilon}^{0*}(\tau, s))$, where $\boldsymbol{C}^*_\tau(\tau, s)$ is an affine modulus tensor, and $\boldsymbol{\varepsilon}^{0*}(\tau, s)$ denotes eigenstrain tensor. Since this linearization form is the same as that of thermo-elastic constitutive laws, the classical thermo-elastic homogenization approaches (e.g., the SC or M−T ones) can be applied to describe the interaction among constituents. Finally, the overall responses of heterogeneous materials in the real-time space are obtained by performing an inverse Laplace's transformation. Although the interaction among different constituents in the microscopic heterogeneous materials is reasonably reflected by this kind of MFH approach, large calculation time during the Laplace's transformation and complex mathematical form restrict its further application.

(2) The approach based on additive interaction law [25-30]. Here, the elastic and viscoplastic deformations of elasto-viscoplastic materials are assumed to occur in two independent time scales, and then the overall response of the materials is split into two different portions (elastic part and viscoplastic one) independent of each other. Thus, the relation among the strain rate $\dot{\boldsymbol{\varepsilon}}$, stress $\boldsymbol{\sigma}$ and stress rate $\dot{\boldsymbol{\sigma}}$ is provided as: $\dot{\boldsymbol{\varepsilon}} = \boldsymbol{C}^{-1} : \dot{\boldsymbol{\sigma}} + \boldsymbol{M} : \boldsymbol{\sigma}$, where $\boldsymbol{C}$ denotes the elasticity tensor and $\boldsymbol{M}$ denotes the viscoplastic tangent (or secant) modulus tensor. Correspondingly, the elasto-viscoplastic inclusion problem is regarded as a superposition of equivalent elastic problem and viscoplastic one. Then, based on this linearization method, the classical elastic homogenization schemes [14] and viscoplastic ones [31] are used to consider the interactions involved in the equivalent elastic problem and viscoplastic one, respectively. This approach has an advantage of low calculation time, but the coupling effect between the elastic deformation and viscoplastic one is not considered. Thus, when the viscosity coefficient of heterogeneous materials is small, its predicted results are very near to the upper bound of solutions if a viscoplastic secant modulus tensor is adopted, while the predicted results are very near to the lower bound of solutions if a viscoplastic tangent modulus tensor is adopted.

(3) The generalized affine linearization (GAL) approach [32-34]. In fact, for elasto-viscoplastic materials, a part of viscoplastic strain cannot respond completely in each loading step due to the limited time. To keep the match of time scales between the elastic response and viscoplastic one, an affine strain increment is introduced. Thus, the elasto-viscoplastic constitutive laws are linearized as follows: (a) the constitutive laws are first discretized based on the Euler's integration algorithm; (b) its main equations are linearized at a loading step, and an affine relationship is given as: $\Delta\boldsymbol{\sigma} = \boldsymbol{C}^{\text{alg}} : (\Delta\boldsymbol{\varepsilon} - \Delta\boldsymbol{\varepsilon}^{\text{af}})$, where $\boldsymbol{C}^{\text{alg}}$ denotes the tangent modulus operator, $\Delta\boldsymbol{\varepsilon}^{\text{af}}$ represents the affine strain increment [32]. In fact, this linearization method provides a linear relationship between the stress increment $\Delta\boldsymbol{\sigma}$ and partial responding strain increment $\Delta\boldsymbol{\varepsilon} - \Delta\boldsymbol{\varepsilon}^{\text{af}}$, rather than the stress increment $\Delta\boldsymbol{\sigma}$ and whole strain one $\Delta\boldsymbol{\varepsilon}$; the introduced affine strain increment is the strain corresponding to hysteretic viscoplastic response. This linearization form is the same as that of thermo-elastic constitutive laws, so the linearized constitutive laws are easily implemented into the incremental MFH schemes (e.g., the SC or M−T ones) of thermo-elastic heterogeneous material. This approach not only has a low calculation cost, but also considers the coupling effect between the elastic and viscoplastic deformations. However, the obtained tangent modulus operator always overestimates the interaction among different constituents in the microscopic heterogeneous materials. Correspondingly, the predicted results are stiffer than the corresponding finite element simulations, especially for the heterogeneous materials with large viscosity or subjected to a high strain rate loading [32].

(4) The approach based on incremental variational formulations [35-39]. Here, a so-called linear analogy composite material is defined as a virtual one whose constituents behavior as the linearized ones of real constituents at a given stress–strain state. Then, based on the defined linear relation, a designed variational statement is adopted to estimate the optimal properties which can ensure the values of potential being as close as possible to that at non-uniform stress–strain state. The key point of such approach lies in the definition of linear analogy composite material. Different definitions of linear analogy composites may result in different practicalities of the approaches. Overall, the effectiveness of such approaches in predicting the overall responses of two-phase elasto-viscoplastic composites has been proved; however, the accuracy in modeling the local responses of local phases should be further promoted.

In this work, aiming at the unmatched time scales of elastic and viscoplastic responses in the elasto-viscoplastic microscopic heterogeneous materials, a new incremental secant linearization method is put forward. The linearization relationship between the second-ordered stress increment $\Delta\boldsymbol{\sigma}$ and strain increment $\Delta\boldsymbol{\varepsilon}$ tensors is given as: $\Delta\boldsymbol{\sigma} = \boldsymbol{C}^{\text{sec}} : \Delta\boldsymbol{\varepsilon}$, where $\boldsymbol{C}^{\text{sec}}$ is the four-ordered incremental secant modulus tensor. After the new secant linearization method is implemented into the M−T and SC approaches, the stress-stress curves of different elasto-viscoplastic microscopic heterogeneous materials (i.e., the composite and polycrystalline materials) under different loading conditions are predicted. By comparing the predicted results with those obtained by the finite element method (FEM), fast Fourier's transformation (FFT) method and generalized affine linearization (GAL) based homogenization approaches, it is shown that the new secant linearization can take an important role in the effective and accurate simulations of correspondent overall responses of elasto-viscoplastic microscopic heterogeneous materials.

1.1. Incremental secant linearization method

The key issue in linearizing an elasto-viscoplastic constitutive law is how to deal with the unmatched time scales between the elastic and viscoplastic deformations. Here, a new linearization method is developed by reasonably handling such unmatched time scales involved in elasto-viscoplastic constitutive models. This new linearization method consists of three steps: (1) based on the Taylor's expansion of a general form of stress increment function, a linearization equation among the strain increment, time increment and stress increment is constructed; (2) based on the Hooke's law, another linearization equation among the strain increment, time increment and stress increment is provided; (3) a linearization relationship between the stress increment and strain increment is obtained by solving such two equations. The mathematical description of new linearization approach is given as follows:

For elasto-viscoplastic materials, the main constitutive equations are given as the following general forms:

$$\dot{\boldsymbol{\varepsilon}} = \dot{\boldsymbol{\varepsilon}}^{\mathrm{e}} + \dot{\boldsymbol{\varepsilon}}^{\mathrm{vp}} \tag{1a}$$

$$\dot{\boldsymbol{\sigma}} = \boldsymbol{C} : \dot{\boldsymbol{\varepsilon}}^{\mathrm{e}} \tag{1b}$$

$$\dot{\boldsymbol{\varepsilon}}^{\mathrm{vp}} = \tilde{\boldsymbol{\varepsilon}}^{\mathrm{p}}(\boldsymbol{\sigma}, \boldsymbol{V}) \tag{1c}$$

$$\dot{\boldsymbol{V}} = \tilde{\boldsymbol{V}}(\boldsymbol{\sigma}, \dot{\boldsymbol{\varepsilon}}^{\mathrm{vp}}, \boldsymbol{V}) \tag{1d}$$

where $\dot{\boldsymbol{\varepsilon}}$ and $\dot{\boldsymbol{\sigma}}$ denote the strain and stress rate tensors, respectively; $\dot{\boldsymbol{\varepsilon}}^{\mathrm{e}}$ and $\dot{\boldsymbol{\varepsilon}}^{\mathrm{vp}}$, respectively, represent the elastic and viscoplastic strain rate tensors. $\boldsymbol{C}$ denotes the elasticity tensor, and $\boldsymbol{V}$ represents a collection of all concerned internal variables, which generally contain the scalar, vector and/or tensor variables. $\tilde{\boldsymbol{\varepsilon}}^{\mathrm{p}}$ and $\tilde{\boldsymbol{V}}$ are the functions defining the evolutions of $\boldsymbol{\varepsilon}^{\mathrm{vp}}$ and $\boldsymbol{V}$, respectively.

Consider the time interval $[t_{\mathrm{n}}, t_{\mathrm{n}+1}]$, and assume that the values of such variables at the time t_{n} have been known. Here, the increments would be expressed by the symbol Δ, i.e., $\Delta t_{\mathrm{n}+1} = t_{\mathrm{n}+1} - t_{\mathrm{n}}$. If the strain and time increments are given, the corresponding stress increment $\Delta\boldsymbol{\sigma}_{\mathrm{n}+1}$ is determinable for stable materials. Then, based on the above generalized elastic-viscoplastic constitutive laws (a detailed derivation process for this equation is given in Appendix B1), the function relation between the stress increment $\Delta\boldsymbol{\sigma}_{\mathrm{n}+1}$ and the strain increment $\Delta\boldsymbol{\varepsilon}_{\mathrm{n}+1}$ and time increment $\Delta t_{\mathrm{n}+1}$ can be given as

$$\Delta\boldsymbol{\sigma}_{\mathrm{n}+1} = \tilde{\boldsymbol{\sigma}}(\Delta\boldsymbol{\varepsilon}_{\mathrm{n}+1}, \boldsymbol{\sigma}_{\mathrm{n}}, \boldsymbol{V}_{\mathrm{n}}, \Delta t_{\mathrm{n}+1}) \tag{2}$$

It is seen that the stress increment $\Delta\boldsymbol{\sigma}_{\mathrm{n}+1}$ depends not only on the strain increment $\Delta\boldsymbol{\varepsilon}_{\mathrm{n}+1}$, but also on the time increment $\Delta t_{\mathrm{n}+1}$. This implies that $\Delta\boldsymbol{\sigma}_{\mathrm{n}+1} \neq \frac{\partial\Delta\boldsymbol{\sigma}_{\mathrm{n}+1}}{\partial\Delta\boldsymbol{\varepsilon}_{\mathrm{n}+1}} : \Delta\boldsymbol{\varepsilon}_{\mathrm{n}+1}$, since $\Delta t_{\mathrm{n}+1}$ should not be 0 in each loading step.

The initial condition of Eq. (2) can be given as

$$\mathbf{0} = \tilde{\boldsymbol{\sigma}}(\mathbf{0}, \boldsymbol{\sigma}_{\mathrm{n}}, \boldsymbol{V}_{\mathrm{n}}, 0) \tag{3}$$

which implies that the stress increment $\Delta\boldsymbol{\sigma}_{\mathrm{n}+1}$ is zero once the strain increment $\Delta\boldsymbol{\varepsilon}_{\mathrm{n}+1}$ and time increment $\Delta t_{\mathrm{n}+1}$ are zero. In some special loading cases (i.e., constant applied loading rates), the strain increment may have a complex function relationship with the time increment in a time interval. However, based on the invariance of total differential forms, it is reasonable to only differentiate the explicit variables in equation without distinguishing the relationship among the variables. Thus, adopting the Taylor's expansion of stress incremental function at the point $\tilde{\boldsymbol{\sigma}}(\Delta\boldsymbol{\varepsilon}_{\mathrm{n}+1}, \boldsymbol{\sigma}_{\mathrm{n}}, \boldsymbol{V}_{\mathrm{n}}, \Delta t_{\mathrm{n}+1})$, the value of $\tilde{\boldsymbol{\sigma}}(\mathbf{0}, \boldsymbol{\sigma}_{\mathrm{n}}, \boldsymbol{V}_{\mathrm{n}}, 0)$ can be expressed as

$$\begin{aligned}\mathbf{0} = \tilde{\boldsymbol{\sigma}}(\mathbf{0}, \boldsymbol{\sigma}_{\mathrm{n}}, \boldsymbol{V}_{\mathrm{n}}, 0) = \Delta\boldsymbol{\sigma}_{\mathrm{n}+1} + \tfrac{\partial\Delta\boldsymbol{\sigma}_{\mathrm{n}+1}}{\partial\Delta\boldsymbol{\varepsilon}_{\mathrm{n}+1}}(\mathbf{0} - \Delta\boldsymbol{\varepsilon}_{\mathrm{n}+1}) + \tfrac{\partial\Delta\boldsymbol{\sigma}_{\mathrm{n}+1}}{\partial\boldsymbol{\sigma}_{\mathrm{n}}}(\boldsymbol{\sigma}_{\mathrm{n}} - \boldsymbol{\sigma}_{\mathrm{n}}) + \\ \tfrac{\partial\Delta\boldsymbol{\sigma}_{\mathrm{n}+1}}{\partial\boldsymbol{V}_{\mathrm{n}}}(\boldsymbol{V}_{\mathrm{n}} - \boldsymbol{V}_{\mathrm{n}}) + \tfrac{\partial\Delta\boldsymbol{\sigma}_{\mathrm{n}+1}}{\partial\Delta t_{\mathrm{n}+1}}(0 - \Delta t_{\mathrm{n}+1}) + o(\mathbf{0} - \Delta\boldsymbol{\varepsilon}_{\mathrm{n}+1}, \mathbf{0}, \mathbf{0}, 0 - \Delta t_{\mathrm{n}+1})\end{aligned} \tag{4}$$

where, $o(\mathbf{0} - \Delta\boldsymbol{\varepsilon}_{\mathrm{n}+1}, \mathbf{0}, \mathbf{0}, \Delta t_{\mathrm{n}+1})$ is an infinitesimal quantity.

It can be obtained from Eq. (4) that

$$\Delta\boldsymbol{\sigma}_{\mathrm{n}+1} = \frac{\partial\Delta\boldsymbol{\sigma}_{\mathrm{n}+1}}{\partial\Delta\boldsymbol{\varepsilon}_{\mathrm{n}+1}} : \Delta\boldsymbol{\varepsilon}_{\mathrm{n}+1} + \frac{\partial\Delta\boldsymbol{\sigma}_{\mathrm{n}+1}}{\partial\Delta t_{\mathrm{n}+1}}\Delta t_{\mathrm{n}+1} - o(\mathbf{0} - \Delta\boldsymbol{\varepsilon}_{\mathrm{n}+1}, \mathbf{0}, \mathbf{0}, 0 - \Delta t_{\mathrm{n}+1}) \tag{5}$$

By neglecting the second-ordered infinitesimal quantity, a linearized equation among the stress increment $\Delta\boldsymbol{\sigma}_{\mathrm{n}+1}$, strain increment $\Delta\boldsymbol{\varepsilon}_{\mathrm{n}+1}$ and time increment $\Delta t_{\mathrm{n}+1}$ is obtained as:

$$\Delta\boldsymbol{\sigma}_{\mathrm{n}+1} \approx \frac{\partial\Delta\boldsymbol{\sigma}_{\mathrm{n}+1}}{\partial\Delta\boldsymbol{\varepsilon}_{\mathrm{n}+1}} : \Delta\boldsymbol{\varepsilon}_{\mathrm{n}+1} + \frac{\partial\Delta\boldsymbol{\sigma}_{\mathrm{n}+1}}{\partial\Delta t_{\mathrm{n}+1}}\Delta t_{\mathrm{n}+1} \tag{6}$$

It should be noted that the term $\frac{\partial\Delta\boldsymbol{\sigma}_{\mathrm{n}+1}}{\partial\Delta t_{\mathrm{n}+1}}\Delta t_{\mathrm{n}+1}$ denotes the hysteretic response of viscoplastic materials with respect to time. Generally, the hysteretic response resulting from the viscoplastic deformation always leads to a stress relaxation. Thus, the term $\frac{\partial\Delta\boldsymbol{\sigma}_{\mathrm{n}+1}}{\partial\Delta\boldsymbol{\varepsilon}_{\mathrm{n}+1}} : \Delta\boldsymbol{\varepsilon}_{\mathrm{n}+1}$ is always larger than $\Delta\boldsymbol{\sigma}_{\mathrm{n}+1}$.

Moreover, based on the Hooke's law, another equation among $\Delta\boldsymbol{\sigma}_{\mathrm{n}+1}$, $\Delta\boldsymbol{\varepsilon}_{\mathrm{n}+1}$ and $\Delta t_{\mathrm{n}+1}$ can be obtained as

$$\Delta\boldsymbol{\sigma}_{\mathrm{n}+1} = \boldsymbol{C} : \left(\Delta\boldsymbol{\varepsilon}_{\mathrm{n}+1} - \frac{\Delta\boldsymbol{\varepsilon}^{\mathrm{vp}}_{\mathrm{n}+1}}{\Delta t_{\mathrm{n}+1}}\Delta t_{\mathrm{n}+1}\right) \tag{7}$$

By Eqs. (6) and (7), a linearized equation for the stress increment $\Delta\boldsymbol{\sigma}_{\mathrm{n}+1}$ with respect to the strain increment $\Delta\boldsymbol{\varepsilon}_{\mathrm{n}+1}$ is easily obtained as follows:

Let $\boldsymbol{p}_{\mathrm{n}+1}$ be the direction tensor of $\frac{\partial\Delta\boldsymbol{\sigma}_{\mathrm{n}+1}}{\partial\Delta t_{\mathrm{n}+1}}$ and $\boldsymbol{q}_{\mathrm{n}+1}$ be the direction tensor of $\boldsymbol{C} : \frac{\Delta\boldsymbol{\varepsilon}^{\mathrm{vp}}_{\mathrm{n}+1}}{\Delta t_{\mathrm{n}+1}}$, then the following equation can be obtained:

$$\frac{\partial\Delta\boldsymbol{\sigma}_{\mathrm{n}+1}}{\partial\Delta t_{\mathrm{n}+1}} = \Phi_{\mathrm{n}+1}\boldsymbol{p}_{\mathrm{n}+1} \otimes \boldsymbol{q}_{\mathrm{n}+1} : \boldsymbol{C} : \frac{\Delta\boldsymbol{\varepsilon}^{\mathrm{vp}}_{\mathrm{n}+1}}{\Delta t_{\mathrm{n}+1}} \tag{8}$$

$$\Phi_{\mathrm{n}+1} = \frac{\left\| \frac{\partial\Delta\boldsymbol{\sigma}_{\mathrm{n}+1}}{\partial\Delta t_{\mathrm{n}+1}} \right\|}{\left\| \boldsymbol{C} : \frac{\Delta\boldsymbol{\varepsilon}^{\mathrm{vp}}_{\mathrm{n}+1}}{\Delta t_{\mathrm{n}+1}} \right\|} \tag{9}$$

where $\left\| \frac{\partial\Delta\boldsymbol{\sigma}_{\mathrm{n}+1}}{\partial\Delta t_{\mathrm{n}+1}} \right\|$ and $\left\| \boldsymbol{C} : \frac{\Delta\boldsymbol{\varepsilon}^{\mathrm{vp}}_{\mathrm{n}+1}}{\Delta t_{\mathrm{n}+1}} \right\|$ are the magnitudes of $\frac{\partial\Delta\boldsymbol{\sigma}_{\mathrm{n}+1}}{\partial\Delta t_{\mathrm{n}+1}}$ and $\boldsymbol{C} : \frac{\Delta\boldsymbol{\varepsilon}^{\mathrm{vp}}_{\mathrm{n}+1}}{\Delta t_{\mathrm{n}+1}}$. The direction tensors $\boldsymbol{p}_{\mathrm{n}+1}$ and $\boldsymbol{q}_{\mathrm{n}+1}$ satisfy $\left\| \frac{\partial\Delta\boldsymbol{\sigma}_{\mathrm{n}+1}}{\partial\Delta t_{\mathrm{n}+1}} \right\| \boldsymbol{p}_{\mathrm{n}+1} = \frac{\partial\Delta\boldsymbol{\sigma}_{\mathrm{n}+1}}{\partial\Delta t_{\mathrm{n}+1}}$ and $\left\| \boldsymbol{C} : \frac{\Delta\boldsymbol{\varepsilon}^{\mathrm{vp}}_{\mathrm{n}+1}}{\Delta t_{\mathrm{n}+1}} \right\| \boldsymbol{q}_{\mathrm{n}+1} = \boldsymbol{C} : \frac{\Delta\boldsymbol{\varepsilon}^{\mathrm{vp}}_{\mathrm{n}+1}}{\Delta t_{\mathrm{n}+1}}$.

Thus, combining Eqs. (6) with (7) (a detailed derivation process for this equation is given in Appendix B2), it yields

$$\left(\boldsymbol{I} + \Phi_{\mathrm{n}+1}\boldsymbol{p}_{\mathrm{n}+1} \otimes \boldsymbol{q}_{\mathrm{n}+1}\right) : \Delta\boldsymbol{\sigma}_{\mathrm{n}+1} = \left(\frac{\partial\Delta\boldsymbol{\sigma}_{\mathrm{n}+1}}{\partial\Delta\boldsymbol{\varepsilon}_{\mathrm{n}+1}} + \Phi_{\mathrm{n}+1}\boldsymbol{p}_{\mathrm{n}+1} \otimes \boldsymbol{q}_{\mathrm{n}+1} : \boldsymbol{C}\right) : \Delta\boldsymbol{\varepsilon}_{\mathrm{n}+1} \tag{10}$$

where $\boldsymbol{I}$ is the fourth-order unit tensor.

If the tensor $\boldsymbol{I} + \Phi_{\mathrm{n}+1}\boldsymbol{p}_{n+1} \otimes \boldsymbol{q}_{n+1}$ is reversible, then

$$\Delta\boldsymbol{\sigma}_{\mathrm{n}+1} = \boldsymbol{C}^{\mathrm{sec}}_{\mathrm{n}+1} : \Delta\boldsymbol{\varepsilon}_{\mathrm{n}+1} \tag{11a}$$

$$\boldsymbol{C}^{\mathrm{sec}}_{\mathrm{n}+1} = \left(\boldsymbol{I} + \Phi_{\mathrm{n}+1}\boldsymbol{p}_{\mathrm{n}+1} \otimes \boldsymbol{q}_{\mathrm{n}+1}\right)^{-1} : \left(\frac{\partial\Delta\boldsymbol{\sigma}_{\mathrm{n}+1}}{\partial\Delta\boldsymbol{\varepsilon}_{\mathrm{n}+1}} + \Phi_{\mathrm{n}+1}\boldsymbol{p}_{\mathrm{n}+1} \otimes \boldsymbol{q}_{\mathrm{n}+1} : \boldsymbol{C}\right) \tag{11b}$$

where $\boldsymbol{C}^{\mathrm{sec}}_{\mathrm{n}+1}$ is the new proposed incremental secant modulus tensor. Eq. (11a) is the linearized equation between the stress increment $\Delta\boldsymbol{\sigma}_{\mathrm{n}+1}$ and strain increment $\Delta\boldsymbol{\varepsilon}_{\mathrm{n}+1}$.

To sum up, by effectively dealing with the unmatched time scales between the elastic and viscoplastic deformations, a new incremental secant linearization method is developed in this work. Recently, Wu et al. [40] also developed an incremental secant method for elasto-viscoplastic composites. However, different from Wu et al. [40], the proposed new linearization method regards the time increment as an independent variable which plays the same role as does the strain

increment. Furthermore, the linearized equation for the elasto-plastic constitutive model is given as $\Delta\boldsymbol{\sigma}_{n+1} = \boldsymbol{C}^{alg}_{n+1} : \Delta\boldsymbol{\varepsilon}_{n+1}$; comparing it with Eq. (11a), it is readily found that the linearization form of elasto-viscoplastic constitutive model provided by the newly proposed method is the same as that of elasto-plastic constitutive one. In fact, such an incremental secant modulus tensor $\boldsymbol{C}^{sec}_{n+1}$ can be reduced to the algorithmic tangent operator $\boldsymbol{C}^{alg}_{n+1}$ if the rate dependence can be neglected (which means $\Phi = 0$). This implies that the incremental secant linearization method can be regarded as an extended version of the elasto-plastic tangent one.

2. Incremental secant linearization-based homogenization approaches

Since the M−T and SC approaches can reasonably provide the relationship between the mechanical responses of heterogeneous materials and the local ones of each constituent, they are widely used to describe the mechanical responses of microscopic heterogeneous materials [7,17,25,26,41,42]. Here, the newly proposed linearization method is implemented into the M−T and SC homogenization approaches to describe the deformations of elasto-viscoplastic composite and polycrystalline materials, respectively, and then the effectiveness and accuracy of the new linearization method can be validated.

2.1. Incremental secant linearization-based Mori-Tanaka's approach

For simplicity, we only focus on the two-phase composites, i.e., a matrix phase and an inclusion one. It should be noted that only the main equations of incremental secant linearization-based Mori-Tanaka's approach are provided (the detailed deducing procedures can be found in the Appendix B1) as follows:

$$\langle\Delta\boldsymbol{\varepsilon}_{n+1}\rangle_M = \boldsymbol{B}_{n+1} : \langle\Delta\boldsymbol{\varepsilon}_{n+1}\rangle_I \tag{12a}$$

$$\langle\Delta\boldsymbol{\varepsilon}_{n+1}\rangle_I = [(1-f)\boldsymbol{B}_{n+1} + f\boldsymbol{I}]^{-1} : \Delta\bar{\boldsymbol{\varepsilon}}_{n+1} \tag{12b}$$

$$\boldsymbol{B}_{n+1} = \boldsymbol{S}_{n+1} : \left[\left(\boldsymbol{C}^{sec}_{n+1}\right)_M\right]^{-1} : \left[\left(\boldsymbol{C}^{sec}_{n+1}\right)_I - \left(\boldsymbol{C}^{sec}_{n+1}\right)_M\right] + \boldsymbol{I} \tag{12c}$$

$$\begin{aligned}\bar{\boldsymbol{C}}^{sec}_{n+1} &= (1-f)\left[\boldsymbol{C}^{sec}_{n+1}\right]_M : \boldsymbol{B}_{n+1} : [(1-f)\boldsymbol{B}_{n+1} + f\boldsymbol{I}]^{-1} + \\ &\quad f\left[\boldsymbol{C}^{sec}_{n+1}\right]_I : [(1-f)\boldsymbol{B}_{n+1} + f\boldsymbol{I}]^{-1}\end{aligned} \tag{12d}$$

$$\Delta\bar{\boldsymbol{\sigma}}_{n+1} = \bar{\boldsymbol{C}}^{sec}_{n+1} : \Delta\bar{\boldsymbol{\varepsilon}}_{n+1} \tag{12e}$$

where, $\langle\Delta\boldsymbol{\varepsilon}_{n+1}\rangle_M$ and $\langle\Delta\boldsymbol{\varepsilon}_{n+1}\rangle_I$ are the local volume averaged strain increments, and $\left(\boldsymbol{C}^{sec}_{n+1}\right)_M$ and $\left(\boldsymbol{C}^{sec}_{n+1}\right)_I$ are the incremental secant modulus tensors of matrix and inclusion, respectively; f is the volume fraction of inclusion phase, $\boldsymbol{S}_{n+1}$ is the Eshelby's tensor [43]; $\Delta\bar{\boldsymbol{\varepsilon}}_{n+1}$ and $\Delta\bar{\boldsymbol{\sigma}}_{n+1}$ are the overall strain and stress increments, and $\bar{\boldsymbol{C}}^{sec}_{n+1}$ is the equivalent incremental secant modulus tensor of the composites.

2.2. Incremental secant linearization-based self-consistent approach

It is assumed that each phase in the polycrystalline aggregates obeys an elastic-viscoplastic constitutive law. After linearization, the incremental secant linearization-based self-consistent approach is given in this section. It should be noted that the detailed deducing procedures can be found in the Appendix B2, only the main equations are provided as follows:

$$\langle\Delta\boldsymbol{\varepsilon}_{n+1}\rangle_I = \boldsymbol{B}_I : \Delta\bar{\boldsymbol{\varepsilon}}_{n+1} \tag{13a}$$

$$\boldsymbol{B}_I = \left[\boldsymbol{S}_{n+1} : \left(\bar{\boldsymbol{C}}^{sec}_{n+1}\right)^{-1} : \left(\boldsymbol{C}^{sec}_{n+1}\right)_I - (\boldsymbol{S}_{n+1} - \boldsymbol{I})\right]^{-1} \tag{13b}$$

$$\bar{\boldsymbol{C}}^{sec}_{n+1} = \sum_{I=1}^{n} f_I \left(\boldsymbol{C}^{sec}_{n+1}\right)_I : \boldsymbol{B}_I \tag{13c}$$

$$\Delta\bar{\boldsymbol{\sigma}}_{n+1} = \bar{\boldsymbol{C}}^{sec}_{n+1} : \Delta\bar{\boldsymbol{\varepsilon}}_{n+1} \tag{13d}$$

where, $\langle\Delta\boldsymbol{\varepsilon}_{n+1}\rangle_I$ is the volume averaged strain increment of each phase, $\left(\boldsymbol{C}^{sec}_{n+1}\right)_I$ is the incremental secant modulus tensors of each phase; f is the volume fraction of inclusion phase, $\boldsymbol{S}_{n+1}$ is the Eshelby's tensor [43]; $\Delta\bar{\boldsymbol{\varepsilon}}_{n+1}$ and $\Delta\bar{\boldsymbol{\sigma}}_{n+1}$ are the overall strain and stress increments, and $\bar{\boldsymbol{C}}^{sec}_{n+1}$ is the equivalent incremental secant modulus tensor of heterogeneous materials.

3. Validation and discussion

In this section, the effectiveness of new incremental secant linearization method in modeling the deformations of microscopic heterogeneous materials is validated. The predictions involve different monotonic tensile and non-monotonic/non-radial loading conditions. As we know, the effectiveness of FFT method and FEM in modeling the mechanical responses of the heterogeneous materials characterized by a reasonable representative volume element (RVE) has been proved in many existing references [22,39]. Thus, a comparison of predicted results by the newly developed incremental linearization-based M−T and SC approaches with that obtained by the FEM or FFT methods is conducted to validate the effectiveness of new incremental secant linearization method in predicting the elasto-viscoplastic deformation of microscopic heterogeneous materials.

3.1. Particle-reinforced composites under monotonic loading conditions

In this section, the spherical particle reinforced elasto-viscoplastic composites are adopted as representative ones. Following Pierard et al. [44], a unified elasto-viscoplastic constitutive model is used to describe the elasto-viscoplastic deformations of matrix and inclusion phases in the composites. It should be noted that the constitutive model adopted in Ref. [44] doesn't involve the kinematic hardening term. Here, to make the constitutive model be more universal, a back stress term is introduced to reflect the kinematic hardening. Main equations of such an elasto-viscoplastic constitutive model and the derivation of the incremental secant modulus are provided in Appendix C.

Furthermore, to highlight the advantage of incremental secant linearization method more clearly, the predictions are also compared with these obtained by the M−T approach based on the GAL method. So, the material parameters used in the predictions are consistent with that in Ref. [44] for a particle reinforced composite material.

The C3D8 element of ABAQUS code [45] is adopted, and the element and node numbers of RVE (f = 10%) are 137,320 and 144979, respectively. Fig. 2c shows the finite element mesh for the modeled composites (f = 10%). For simplification, the interfaces between the matrix and inclusion are regarded as being perfect. To impose the monotonic tension, a periodic boundary condition is applied to the RVE, i.e.

$$\begin{aligned}&\boldsymbol{v}(x_1, x_2, 0) - \boldsymbol{v}_3 = \boldsymbol{v}(x_1, x_2, L).\\ &\boldsymbol{v}(x_1, 0, x_3) - \boldsymbol{v}_2 = \boldsymbol{v}(x_1, L, x_3).\\ &\boldsymbol{v}(0, x_1, x_2) - \boldsymbol{v}_1 = \boldsymbol{v}(L, x_1, x_2).\end{aligned} \tag{14}$$

where $\boldsymbol{v}$ denotes the displacement vector, L is the RVE length. In finite element simulations, a tensile loading is imposed along the x_3-direction. Here, $\boldsymbol{v}_3 = (0, 0, \varepsilon L)$, $\boldsymbol{v}_1 = (v_1, 0, 0)$ and $\boldsymbol{v}_2 = (0, v_2, 0)$, where $\boldsymbol{\varepsilon}$ denotes an imposed strain, v_1 and v_2 are two computable displacements of cubic surfaces with the normal vectors perpendicular to the

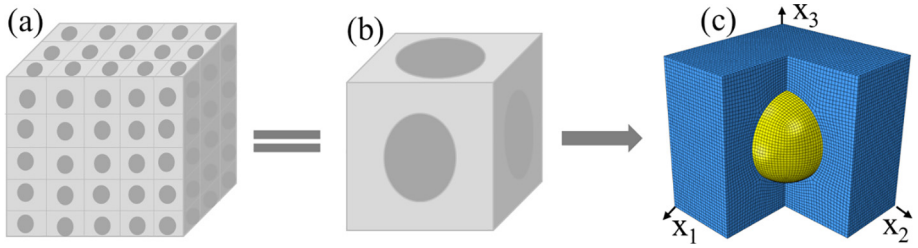

Fig. 1. A model of particle reinforced composite: (a) inclusions embedded into the matrix periodically; (b) representative volume element (RVE); (c) gird for RVE.

x_3-axis. Fig. 1 shows the representative volume element (RVE) for the particle reinforced composites.

Fig. 2 gives the predictions of the composites containing different volume fractions (f = 10%, 20%, 30%, 40% and 50%) of inclusion phase and at a constant strain rate (i.e., $1 \times 10^{-3}\ s^{-1}$); and Table 1 gives all used parameters. It should be noted that the predicted stress responses with large inclusion volume fractions are smaller than the real ones since the M−T method assumes that the remote stress of matrix is equal to its mean stress. To effectively capture the overall mechanical responses of the composites with large inclusion volume fractions, the new linearization method is applied into the extended M−T method developed by Li et al [46] to model the deformation of the composites with large inclusion volume fractions (i.e., 40% and 50%), since the M−T method extended by Li et al. [46] is more suitable for the composite with large inclusion volume fractions. It is seen that the results predicted by the newly developed incremental secant linearization-based M−T approach (denoted as NMT in the figures) agree with correspondent finite element simulations (denoted as FEM in the figures) well, the maximum error between the results predicted by the NMT and FEM is about 2%; while the results predicted by the M−T approach based on a GAL method (denoted as MT in the figures) are stiffer than the finite element simulations. Furthermore, the differences between the predicted results by the finite element simulation and GAL based M−T approach become larger and larger if the inclusion volume fraction increases. Such a deviation can be explained from Fig. 3, which gives the evolution of ratio $\Delta\bar{\varepsilon}_{11}^{af}/\bar{\boldsymbol{M}}:\Delta\bar{\sigma}_{11}$(where $\Delta\bar{\boldsymbol{\varepsilon}}^{af}$, $\Delta\bar{\boldsymbol{\sigma}}$ and $\bar{\boldsymbol{M}}$ are the equivalent affine strain increment, equivalent stress increment and equivalent secant operator for the new incremental secant linearization method or tangent operator for the GAL one of composites, respectively). Fig. 3 shows that at the beginning of tensile deformation, the ratios are equal to zero for the new secant linearization method and GAL one since only elastic deformation exists, i.e., $\Delta\boldsymbol{\varepsilon}^{af}=\mathbf{0}$; however, this ratio for the GAL case increases with the increase of strain and becomes even larger than one after certain viscoplastic deformation. Subsequently, the total strain increment $\Delta\bar{\boldsymbol{\varepsilon}}$ in the GAL method is dominated by $\Delta\bar{\boldsymbol{\varepsilon}}^{af}$, rather than $\bar{\boldsymbol{M}}:\Delta\bar{\boldsymbol{\sigma}}$; moreover, the ratio $\Delta\bar{\varepsilon}_{11}^{af}/\left(\bar{\boldsymbol{M}}:\Delta\bar{\boldsymbol{\sigma}}\right)_{11}$ increases with the decrease of inclusion volume fraction. Thus, the effective compliance tensor derived by the GAL method is so large that the interactions between the matrix and inclusions are overestimated. However, for the newly developed incremental secant linearization method, the ratios $\Delta\bar{\varepsilon}_{11}^{af}/\left(\bar{\boldsymbol{M}}:\Delta\bar{\boldsymbol{\sigma}}\right)_{11}$ keep as zero during the tensile deformation, the interactions between the matrix and inclusions can be effectively predicted by the new linearization-based M−T approach.

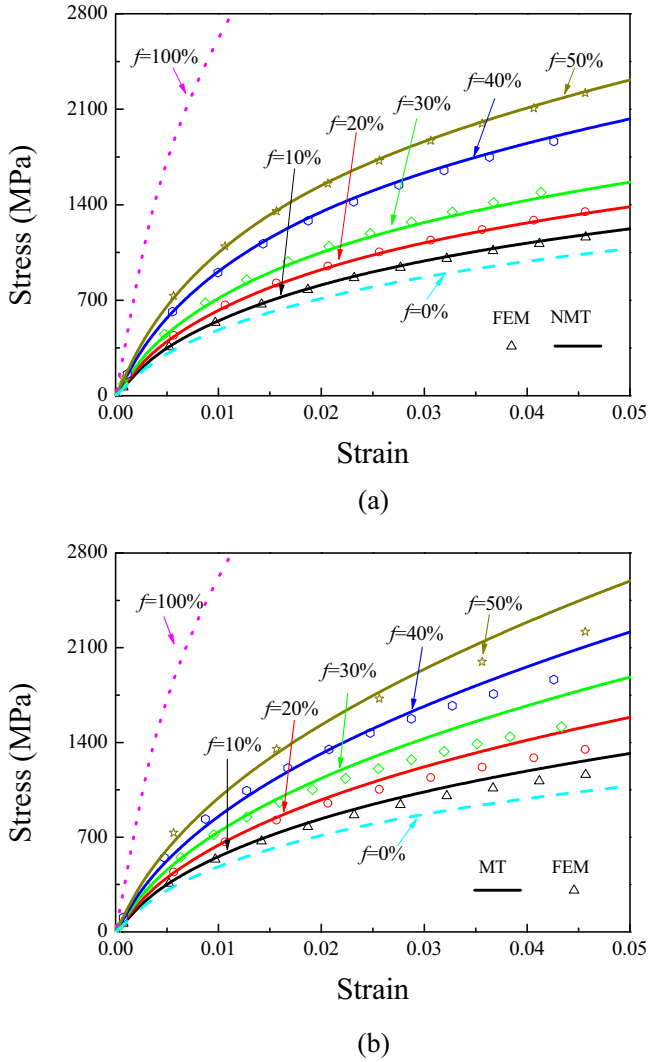

Fig. 2. Tensile stress–strain responses of the composites containing different volume fractions predicted by FEM and M−T approach based on different linearization methods at a strain rate of $10^{-3}\ s^{-1}$; (a) incremental secant linearization one (NMT); (b) the generalized affine linearization one (MT).

To further demonstrate the validity of the newly developed incremental secant linearization method, the monotonic tensile deformations of the composite (f = 20%) at two strain rates (i.e., $1 \times 10^{-3}\ s^{-1}$ and $1 \times 10^{-5}\ s^{-1}$) are also predicted by using the material parameters given in Table 1. Fig. 4 gives the predictions of the composite at different strain rates. It is found from Fig. 4 that the new incremental secant linearization-based M−T approach (i.e., NMT in the figure) can predict the tensile deformations of the composite at different loading rates well. However, the results predicted by the M−T approach based on the GAL method (i.e., MT in the figure) are not very accurate. The differences between the results predicted by the NMT and FEM are less than 2%, while the differences between the results predicted by the MT based on the GAL method and FEM are much larger than 10%. Fig. 5 gives the evolution of ratio $\Delta\bar{\varepsilon}_{11}^{af}/\left(\bar{\boldsymbol{M}}:\Delta\bar{\boldsymbol{\sigma}}\right)_{11}$. It is shown that these ratios are always equal to zero for the M−T approach based on the newly proposed incremental secant linearization method; while the ratios become larger and larger beyond the plastic yielding when

Table 1
Material parameters for the matrix and inclusion of the composites.

Material parameters for the matrix
$E_M = 70$GPa, $\nu_M = 0.33$, $(\gamma_0)_M = 0.0003$
$K_M = 1.5$GPa, $m_M = 50$, $a_M = 0.4$
$R_M = 70$MPa, $h_M = 15$GPa, $\xi_M = 100$
Material parameters for the inclusion
$E_I = 400$GPa, $\nu_I = 0.286$, $(\gamma_0)_I = 0.0002$
$K_I = 8$GPa, $m_I = 50$, $a_I = 0.4$
$R_I = 400$MPa, $h_I = 45$GPa, $\xi_I = 100$

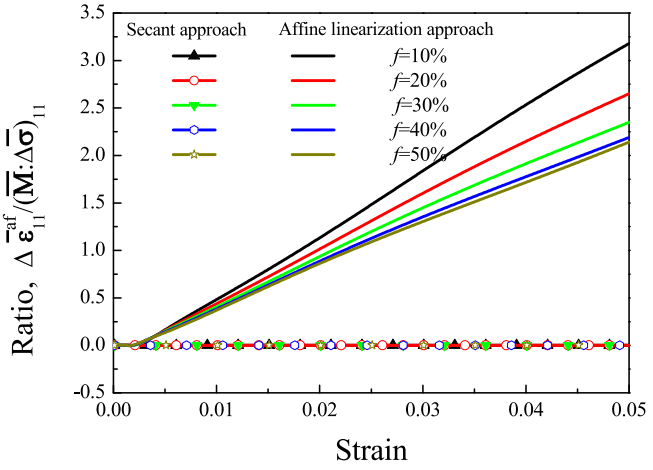

Fig. 3. Evolutions of ratio $\Delta\bar{\varepsilon}^{af}_{11}/\left(\bar{M}:\Delta\bar{\sigma}\right)_{11}$ for the composites with different volume fractions of inclusion in tension at a strain rate of 10^{-3} s^{-1}.

the one based on the GAL method is adopted. This implies that the interaction between the matrix and inclusion is overestimated by the GAL method based M−T approach.

Here, the prediction capabilities of the M−T approaches based on different linearization methods to the overall deformations of elasto-viscoplastic composites with different viscosities are also discussed. The material parameters used in the predictions for the composites with different viscosities have been given in Table 2. Fig. 6 gives the predicted tensile stress–strain curves of the composites (f = 20%) with different viscosities (represented by different values of m_M and m_I) and at a constant strain rate of 1 × 10^{-3} s^{-1}. It is shown that there are almost no differences between the results predicted by the M−T approach based on the incremental secant linearization method and those from FEM, while some significant differences are found in the stress–strain curves predicted by the GAL method based M−T approach and FEM. Fig. 7 shows the evolution of ratio $\Delta\bar{\varepsilon}^{af}_{11}/\left(\bar{M}:\Delta\bar{\sigma}\right)_{11}$. From Fig. 7, it can be found that with the increase of viscosity, the $\Delta\bar{\varepsilon}^{af}_{11}/\left(\bar{M}:\Delta\bar{\sigma}\right)_{11}$ also increases when the GAL method based M−T approach is adopted. This means that the effective compliance tensor derived by the GAL method becomes larger and larger with the increase of $\Delta\bar{\varepsilon}^{af}_{11}/\left(\bar{M}:\Delta\bar{\sigma}\right)_{11}$; the interaction between the matrix and inclusion is less effectively considered by the GAL method when the viscosity of composite is large. Instead, if the NMT is adopted, the interaction between the matrix and inclusion is effectively considered since the effective compliance tensor is accurate (i.e., $\Delta\bar{\varepsilon}^{af}_{11}/\left(\bar{M}:\Delta\bar{\sigma}\right)_{11}$ is always equal to zero).

Also, the deformations of the composites with different hardening moduli (i.e., different K_M and h_M) are predicted by using the material parameters given in Table 3. Fig. 8 gives the predicted results of the composites (f = 20%) with different hardening moduli and at a strain

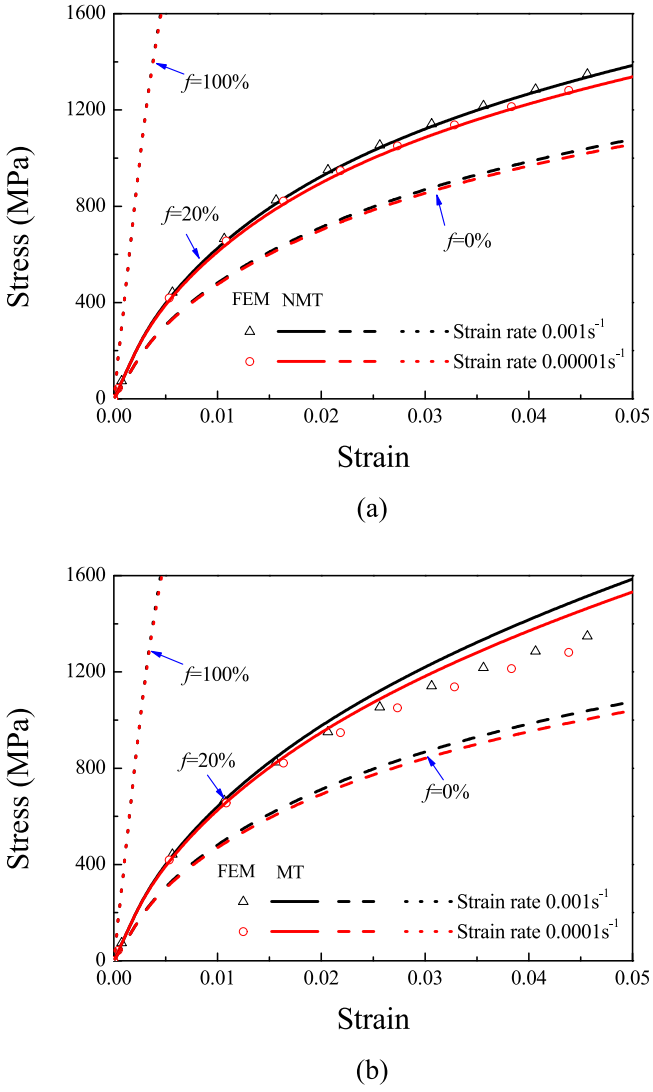

Fig. 4. The stress–strain curves of the composite (f = 20%) predicted by FEM and M−T scheme based on different linearization approaches at different strain rates; (a) incremental secant linearization approach (NMT); (b) the generalized affine linearization method (MT).

rate of 1 × 10^{-3} s^{-1}. It is shown from Fig. 8 that the tensile stress–-strain curves of the composites with different hardening moduli can be well described by the M−T approach based on the new linearization method, the predicted errors are less than 2%; while the tensile curves of the composites with low hardening moduli cannot be accurately predicted by the M−T approach based on the GAL method. Fig. 9 shows the evolutions of the ratio $\Delta\bar{\varepsilon}^{af}_{11}/\left(\bar{M}:\Delta\bar{\sigma}\right)_{11}$. It is indicated from Fig. 9 that the results of the composites with different hardening moduli predicted by the M−T approach based on the new linearization method are always equal to zero, while the ratios predicted by that based on the GAL method are far larger than zero and very sensitive to the variation in the hardening moduli of matrix. If the hardening moduli of matrix are very low, the ratio would be very large, which indicates that the interaction between the matrix and inclusion cannot be effectively considered by the GAL method based M−T approach for the composites with low hardening moduli. However, even if the hardening moduli of matrix are very small, the interaction between the matrix and inclusion is always effectively reflected by the M−T approach based on the newly developed incremental secant linearization method.

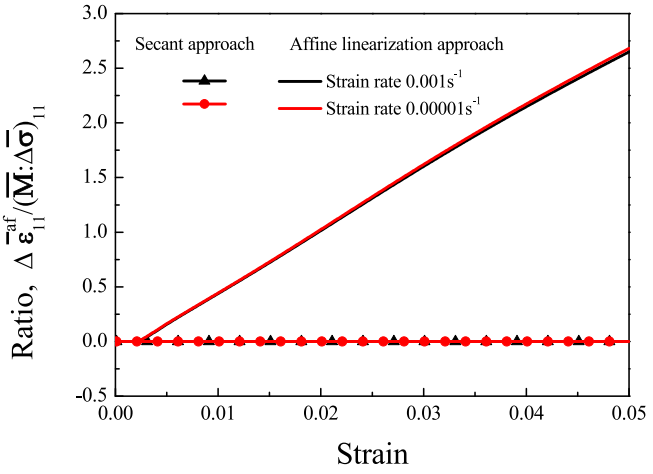

Fig. 5. Evolutions of ratio $\Delta\bar{\varepsilon}_{11}^{af}/\left(\bar{M}:\Delta\bar{\sigma}\right)_{11}$ for the composite ($f = 20\%$) in tension at different strain rates.

Table 2
Material parameters for the matrix and inclusion of the composites with different viscosities.

Material parameters for the matrix
$E_M = 70$GPa, $\nu_M = 0.33$, $(\gamma_0)_M = 0.0003$
$K_M = 1.5$GPa, $\xi_M = 100$, $a_M = 0.4$
$R_M = 70$MPa, $h_M = 15$GPa,
$m_M = 50$ for composite with low viscosity
$m_M = 20$ for composite with medium viscosity
$m_M = 8$ for composite with high viscosity
Material parameters for the inclusion
$E_I = 400$GPa, $\nu_I = 0.286$, $(\gamma_0)_I = 0.0002$
$K_I = 8$GPa, $\xi_I = 100$, $a_I = 0.4$
$R_I = 400$MPa, $h_I = 45$GPa,
$m_I = 50$ for composite with low viscosity
$m_I = 20$ for composite with medium viscosity
$m_I = 8$ for composite with high viscosity

3.2. Particle-reinforced composites under complex loading conditions

To validate the effectiveness of the NMT approach in modeling the deformation of the composites under the non-monotonic loading condition, the deformation of the spherical particle-reinforced composites under the uniaxial cyclic loading condition is predicted by the NMT method at a strain rate of $10^{-3}\,s^{-1}$. And the predicted results are compared with that predicted by FEM, which are provided by Czarnota et al. [47]. The constitutive model for the matrix is the same as that of inclusion, and listed in Appendix C1. The used parameters are listed in Table 4. Fig. 10 gives the overall stress–strain curves of the composites with the inclusion volume fractions of 10% and 25%. From Fig. 10, it can be found that the predictions by the NMT method are in good agreement with the FEM simulations. Fig. 11 provides the correspondent curves of local phases. It is shown that the curves of matrix predicted by the NMT method are also in good agreement with the FEM results; while, for the curves of inclusion, the agreement with the FEM results is not as good. When the volume fraction of inclusion is relatively large (25%), there are some slight discrepancies between the inclusion responses predicted by the FEM and NMT method. The main reason is that the predicted slopes of the inclusion hardening response are lower than those of the FE predictions.

In order to further prove the prediction capability of NMT approach in evaluating the uniaxial cyclic deformation of composites, the cyclic deformation of the composite ($f = 25\%$) with large viscosity and no plastic hardening at the applied strain rates of $5 \times 10^{-3}s^{-1}$ and $5 \times 10^{-5}s^{-1}$ are modeled by the NMT approach. Such results are

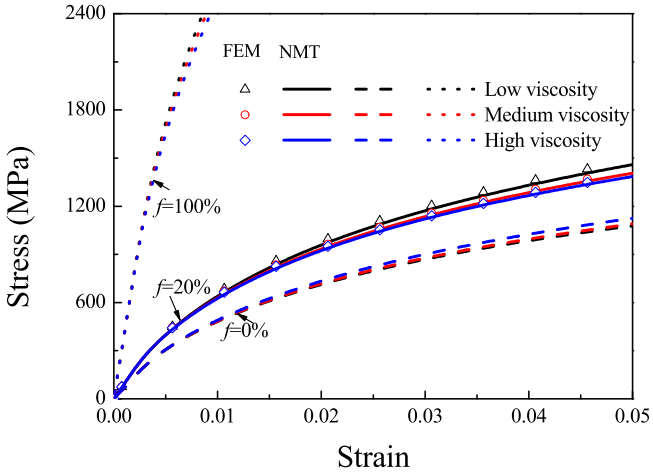

(a)

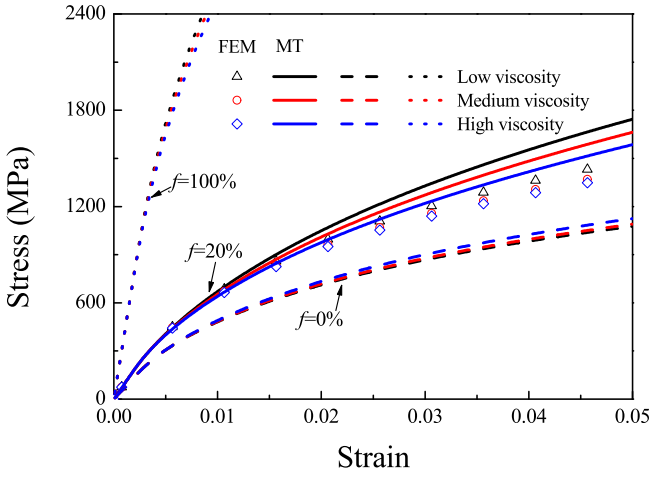

(b)

Fig. 6. The tensile stress–strain responses of the composites ($f = 20\%$) with different viscosities predicted by FEM and M−T scheme based on different linearization methods at a strain rate of $1 \times 10^{-3}\,s^{-1}$; (a) incremental secant linearization approach (NMT); (b) the generalized affine linearization method (MT).

compared with the FFT simulations obtained from Ref. [39]. The constitutive model for the matrix is provided in Appendix D1, and the inclusion is assumed to be elastic. The material parameters used here are given in Table 5. Fig. 12 shows the predicted overall stress–strain curves of composites. From Fig. 12, it can be found that the results predicted by the NMT approach agree with the FFT simulations well. Thus, it can be concluded that the NMT method is effective for the cyclic deformation of composites.

In order to further validate the prediction capability of NMT approach, we also model the deformation of composites subjected to a varied strain in the following function form,

$$\bar{\boldsymbol{\varepsilon}}(t) = \bar{\varepsilon}_{ss}(t)(\boldsymbol{e}_1 \otimes \boldsymbol{e}_3 + \boldsymbol{e}_3 \otimes \boldsymbol{e}_1) + \bar{\varepsilon}_{as}(t)\left(\boldsymbol{e}_1 \otimes \boldsymbol{e}_1 - \frac{1}{2}\boldsymbol{e}_2 \otimes \boldsymbol{e}_2 - \frac{1}{2}\boldsymbol{e}_3 \otimes \boldsymbol{e}_3\right)$$

$$\bar{\varepsilon}_{ss}(t) = \frac{\sqrt{3}}{4}r \cdot [1 - \cos(\omega t)]$$

$$\bar{\varepsilon}_{as}(t) = r \cdot \sin(\omega t) \tag{15}$$

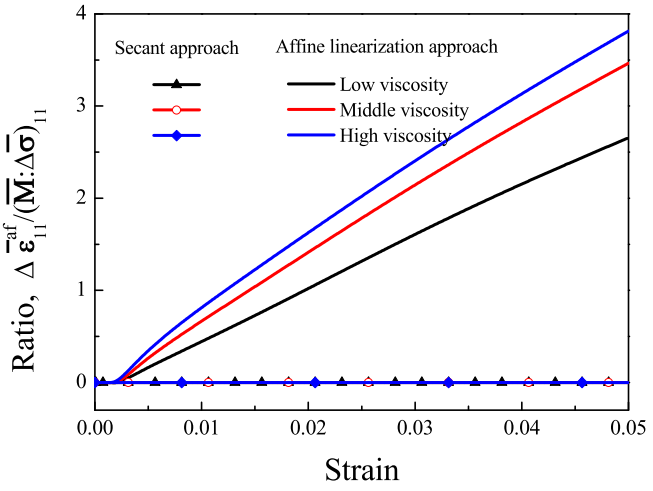

Fig. 7. Evolution of ratio $\Delta\bar{\varepsilon}_{11}^{af}/\left(\bar{\boldsymbol{M}}:\Delta\bar{\boldsymbol{\sigma}}\right)_{11}$ for the composites ($f = 20\%$) with different viscosities during tensile deformation at the strain rate of 1×10^{-3} s^{-1}.

Table 2
Material parameters for the matrix and inclusion of the composites with different viscosities.

Material parameters for the matrix
$E_M = 70$GPa, $\nu_M = 0.33$, $(\gamma_0)_M = 0.0003$
$K_M = 1.5$GPa, $\xi_M = 100$, $a_M = 0.4$
$R_M = 70$MPa, $h_M = 15$GPa,
$m_M = 50$ for composite with low viscosity
$m_M = 20$ for composite with medium viscosity
$m_M = 8$ for composite with high viscosity
Material parameters for the inclusion
$E_I = 400$GPa, $\nu_I = 0.286$, $(\gamma_0)_I = 0.0002$
$K_I = 8$GPa, $\xi_I = 100$, $a_I = 0.4$
$R_I = 400$MPa, $h_I = 45$GPa,
$m_I = 50$ for composite with low viscosity
$m_I = 20$ for composite with medium viscosity
$m_I = 8$ for composite with high viscosity

where $r = 10^{-3}$ and $\omega = \pi/20$ rad/s. The modeled results are compared with the FFT ones provided by Idiart and Lahellec [39]. The constitutive model for the matrix and inclusion is the same as that used in the case shown in Fig. 12. The used parameters are provided in Table 5. Fig. 13 gives the modeled results. From Fig. 13, it can be found that the errors between the results predicted by the NMT and FFT methods are very small, and only the initial yielding cannot be captured very well. This implies that the NMT approach can predict the deformations of composites under complex loading conditions reasonably.

3.3. Polycrystalline materials

To validate the effectiveness of the new increment secant linear method in modeling the deformation of heterogeneous media, the tensile deformation of polycrystalline material at a strain rate of 10^{-3} s^{-1} is also predicted, and the obtained results are compared with the FEM simulation obtained from Ref. [48]. Each grain is assumed to be an FCC crystal, and only the {1 1 1} ⟨1 1 0⟩ slip systems are considered. The main equations of elasto-viscoplastic constitutive model for each grain are provided in Appendix E1, and corresponding incremental secant modulus is deduced in Appendix E2. The material parameters used here are given in Tables 6 and 7, respectively. Fig. 14 shows the stress–strain curve predicted by the SC approach based on the new linearization method (NSC) and FEM. From the comparison, it is seen that the maximum error is about 5%. In fact, the shape of grains used in the FEM simulation is irregular, while that used in the NSC pre-

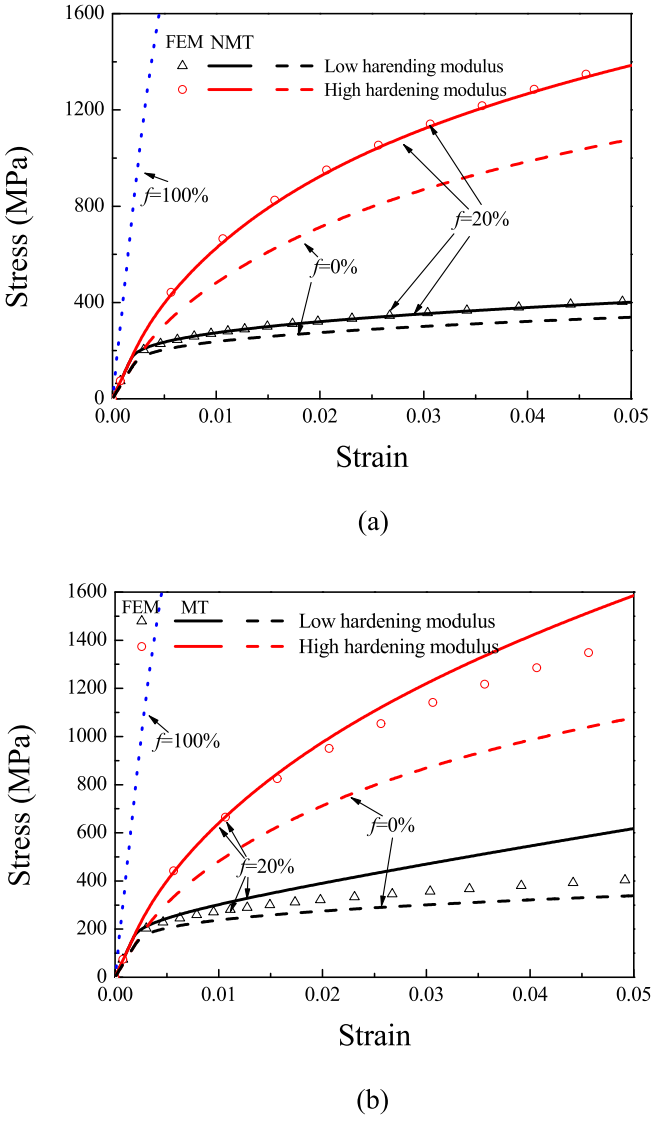

Fig. 8. Tensile stress–strain responses of the composites ($f = 20\%$) with different hardening moduli predicted by FEM and M−T scheme based on different linearization approaches at a strain rate of 1×10^{-3} s^{-1}; (a) incremental secant linearization approach (NMT); (b) the generalized affine linearization method (MT).

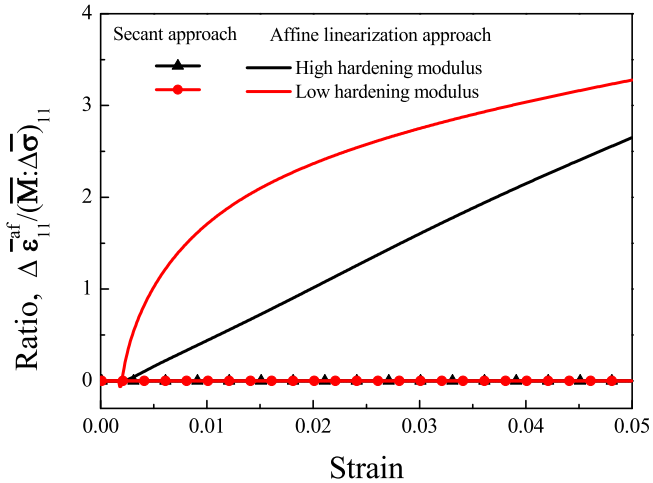

Fig. 9. Evolutions of ratio $\Delta\bar{\varepsilon}_{11}^{af}/\left(\bar{\boldsymbol{M}}:\Delta\bar{\boldsymbol{\sigma}}\right)_{11}$ for the composites ($f = 20\%$) with different hardening moduli in tension at the strain rate of 1×10^{-3} s^{-1}.

Table 4
Material parameters for the composites with no kinematic hardening.

Material parameters for the matrix
$E_M = 100GPa$, $\nu_M = 0.3$, $(\gamma_0)_M = 0.0003$
$\xi_M = 100$, $m_M = 10$, $a_M = 1$
$R_M = 100MPa$, $K_M = 1.5GPa$,$h_M = 0GPa$
Material parameters for the inclusion
$E_I = 500GPa$, $\nu_I = 0.3$, $(\gamma_0)_I = 0.0003$
$K_I = 5GPa$, $m_I = 10$, $a_I = 1$
$R_I = 500MPa$, $h_I = 0GPa$, $\xi_I = 100$

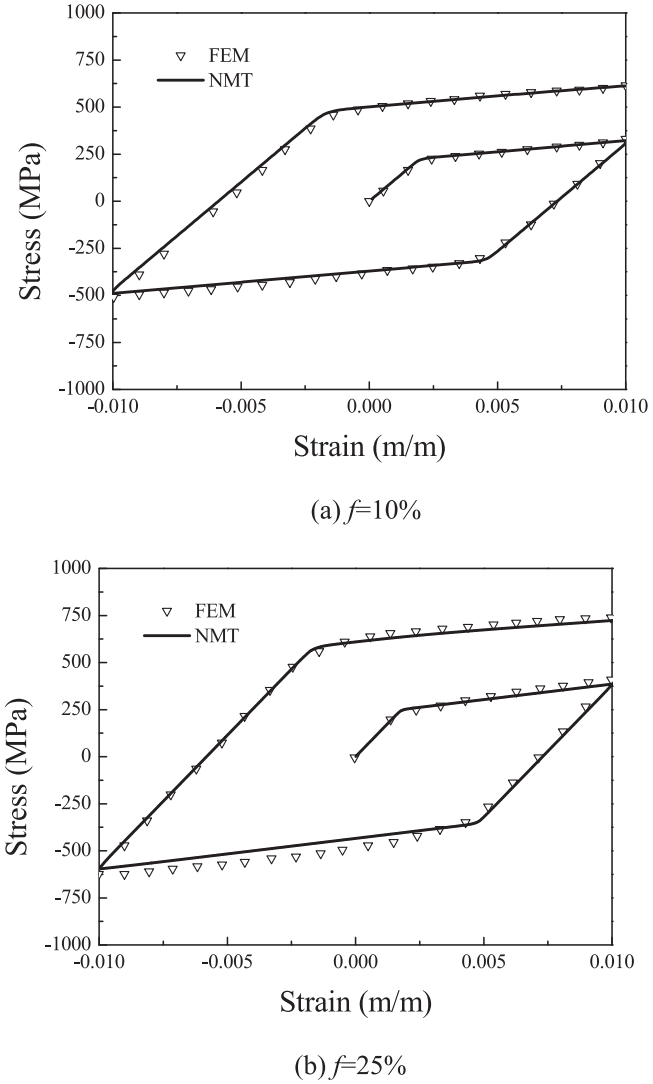

Fig. 10. Overall stress–strain curves of the composites with the inclusion volume fractions of 10% and 25% predicted by the FEM and NMT approach during the monotonic tensile deformation at a strain rate of 10^{-3} s^{-1}. The FEM results are cited from Ref. [47].

diction is regular sphere. It implies that the deformation of heterogeneous media can also be well captured by the increment secant linear method.

3.4. Discussion

3.4.1. Influence of loading step size

Here, the influence of loading step size on the predictions by using the M − T approaches based on different linearization methods is further

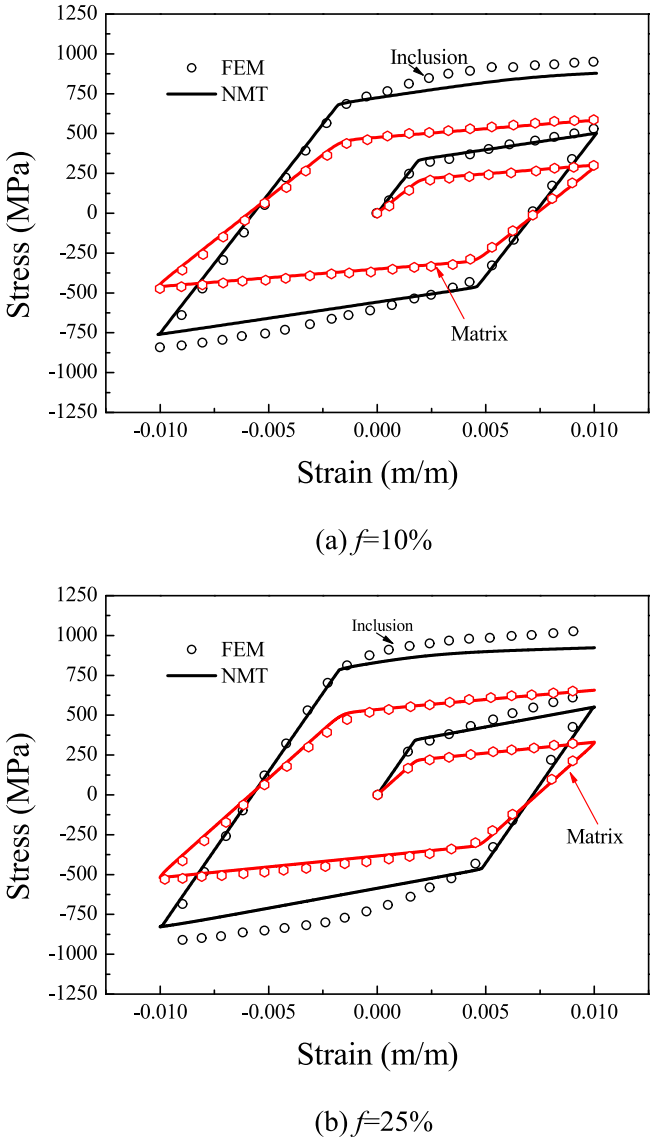

Fig. 11. Phase stress-overall strain curves of the composites with the inclusion volume fractions of 10% and 25% predicted by the FEM and NMT approach during the monotonic tensile deformation at a strain rate of 10^{-3} s^{-1}. The FEM results are cited from Ref. [47].

discussed by adopting the parameters given in Table 1. Fig. 15 shows the predictions to the composite ($f = 10\%$) at a strain rate of 1×10^{-3} s^{-1} and with different loading step sizes. As shown in Fig. 15, the change of loading step size hardly affects the predicted results by the NMT approach, but significantly influences the predicted results by the GAL method based M − T approach. This is because the strain corresponding to the hysteretic viscoplastic response becomes larger and larger with the increase of loading step size. The interaction between the matrix and inclusion is reasonably considered by the new linearization method even if the hysteretic viscoplastic response becomes large, while it is overestimated by the GAL one. Of course, if the size of loading step is not fine enough to capture the short-term and long-term viscoplastic behaviors, the predicted results by the NMT approach also become to be dependent on the size of loading step.

3.4.2. Different choices of Eshelby's tensors

It is well known that the Eshelby's tensor is very important in effectively and accurately describing the interaction between the matrix

Table 5
Material parameters for the composites with no plastic hardening.

Material parameters for the matrix
$\mu_M = 10^3 \cdot \sigma_y$, $\kappa_M \to \infty$, $(\gamma_0)_M = 0.001$
$m_M = 5$,
Material parameters for the inclusion
$\mu_I = 5\mu_M$, $\kappa_I \to \infty$,

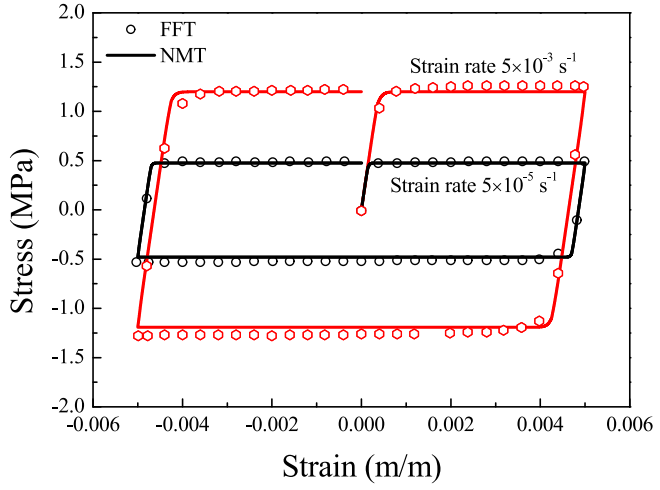

Fig. 12. Overall stress–strain curves of the composites with an inclusion volume fraction of 30% predicted by the FFT and NMT approach during the monotonic tensile deformation at different strain rates. The FFT results are cited from Ref. [39].

and inclusion in the composites. So, different Eshelby's tensors were developed in Refs. [32,49]. However, all these Eshelby's tensors are dependent on the linearization method of nonlinear constitutive model. To further demonstrate the wide applicability of the newly developed incremental secant linearization operator, the tensile deformations of the composites containing different volume fractions of inclusion phase are predicted by the new secant linearization based M−T approach (NMT one) with different Eshelby's tensors, i.e., the isotropic Eshelby's tensor used in the previous subsections of this work (denoted as the isotropic Eshelby's tensor I) [32], isotropic Eshelby's tensor developed by Peng et al. [49] (denoted as the isotropic Eshelby's tensor II) and anisotropic Eshelby's tensor [50]. The material parameters given in Table 1 are used here. Fig. 16 gives the predicted tensile stress–strain curves for the composite at a strain rate of 10^{-3} s^{-1}. It is shown that the stress–strain curves of the composite predicted by the NMT approach with the isotropic Eshelby's tensor I agree with that from the FEM simulations well; the stress values predicted by the NMT approach with the Eshelby's tensor II are only slightly smaller than that from the FEM simulations; while the predictions by using the NMT approach with the anisotropic Eshelby's tensor have large deviation to the FEM simulations. It is in good agreement with the discussion in Ref. [49], and demonstrates that the new incremental secant linearization approach can play a key role in reasonably reflecting the interaction between the matrix and inclusion in the composites, even if different isotropic Eshelby's tensors are chosen.

3.4.3. Effect of linearization form

It is well-known that whether the homogenization approaches can effectively consider the interaction among the constituent phases of composites is determined by the adopted linearization methods for the constitutive models of constituent phases. As commented in the introduction section of this work, the existing linearization methods of elasto-plastic constitutive models can provide a linear relationship

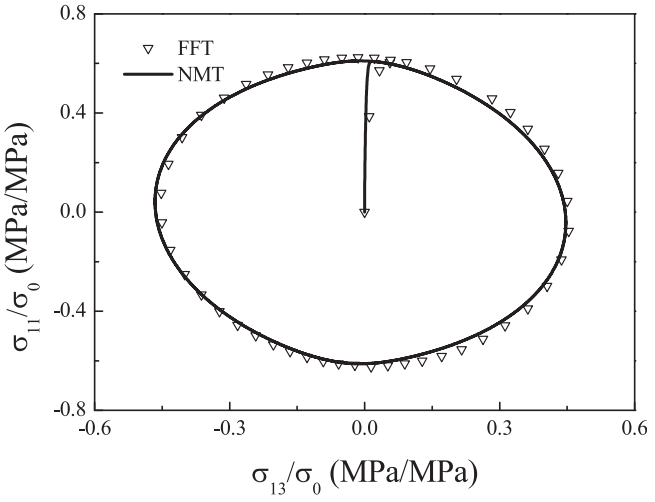

Fig. 13. Overall stress response of the composites with a spherical elastic inclusion under a cyclic loading condition. The FFT result is cited from Ref. [39].

Table 6
Interaction parameters between different slip systems.

Interaction type	Interaction coefficient
Self	1
Coplanar	1
Collinear	0.6
Hirth	12.3
Glissile	1.8
Lomer	1.6

Table 7
Material parameters for single crystal.

$c_{1111} = 197$GPa, $c_{1122} = 125$GPa, $c_{1212} = 122$GPa
$K = 12$MPa, $m = 11$, $r_0 = 40$MPa
$Q = 10$MPa,$B = 3A = 40$GPa
$D = 1.5$GPa

between the stress increment and strain one. Its linearization form has the same mathematical form as the Hooke's law, so the homogenization approaches developed for the linearly elastic composites are easily extended to the elasto-plastic composites. However, the existing linearization methods developed for the elasto-viscoplastic composites cannot always directly give a similar relation between the stress and strain increments. For example, as discussed in the introduction, the approach based on the Laplace's transformation provides a fictitious linear relationship among the stress rate $\dot{\boldsymbol{\sigma}}$, strain rate $\dot{\boldsymbol{\varepsilon}}$ and eigenstrain tensor $\boldsymbol{\varepsilon}^{0*}(\tau, s)$; the approach based on the additive interaction law gives a linear relation among the stress σ, stress rate $\dot{\boldsymbol{\sigma}}$ and strain rate $\dot{\boldsymbol{\varepsilon}}$; and the GAL method gives a linear relation among the stress increment $\Delta\boldsymbol{\sigma}$, strain increment $\Delta\boldsymbol{\varepsilon}$ and affine strain increment $\Delta\boldsymbol{\varepsilon}^{af}$. Thus, the classical thermo-elastic homogenization schemes are used to estimate the interaction among the different constituents of elasto-viscoplastic composites if the approach based on the Laplace's transformation or the GAL method is adopted; classical elastic homogenization schemes and viscoplastic ones have to be used to consider the interaction between the equivalent elastic problem and viscoplastic one, respectively. It implies that the relation between the elasto-plastic homogenization method and elasto-viscoplastic ones is cut off if the

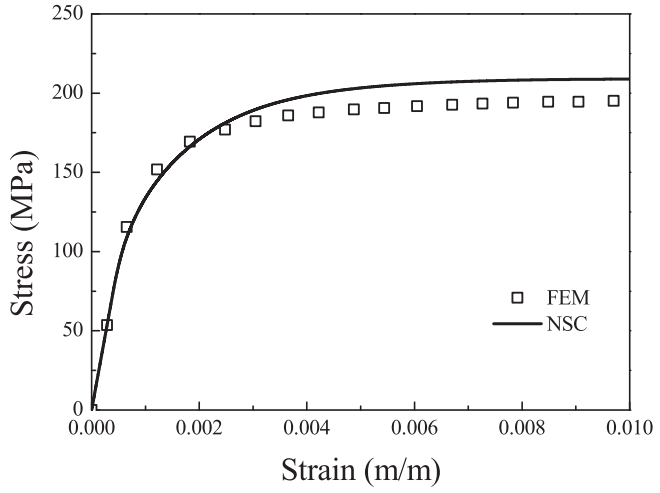

Fig. 14. Stress–strain curves of polycrystalline aggregates predicted by FEM and NSC approach during tensile deformation at a strain rate of $10^{-3}\,s^{-1}$. The FEM results are cited from Ref. [48].

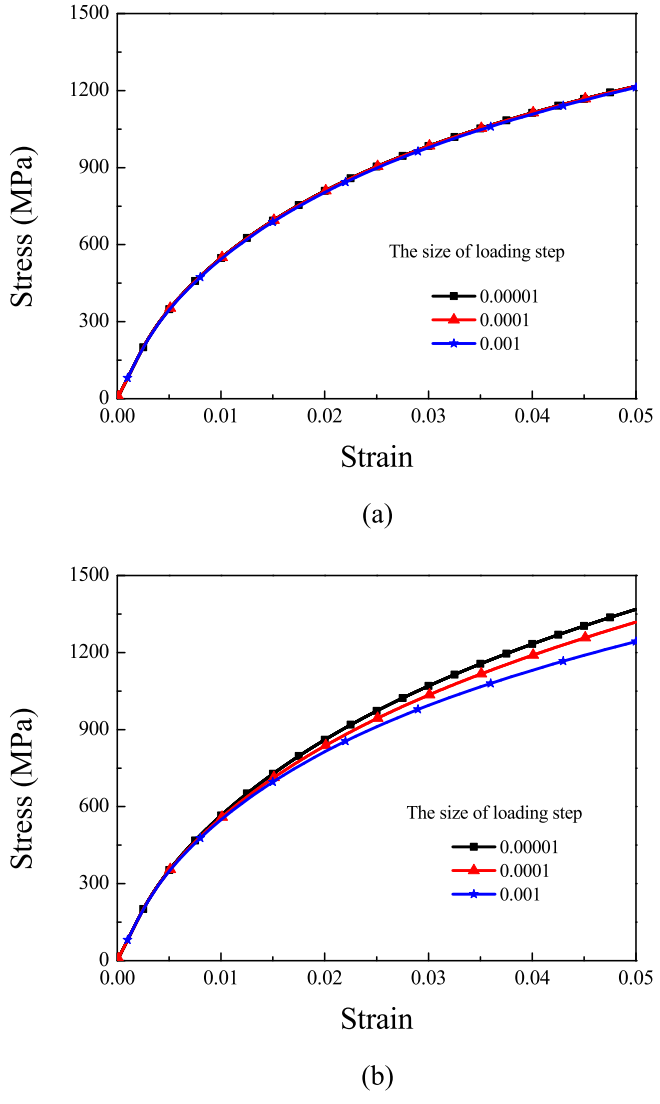

Fig. 15. Tensile stress–strain curves of the composites ($f = 10\%$) predicted by the M−T approaches based on different linearization methods at different sizes of loading step; (a) new incremental secant linearization approach (NMT); (b) generalized affine linearization method (MT).

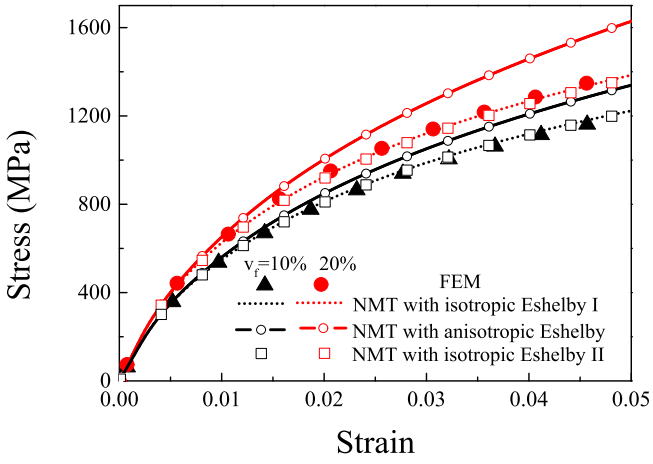

Fig. 16. Stress–strain curves of the composites containing different volume fractions predicted by FEM and the NMT approach with different Eshelby tensors at the strain rate of $1 \times 10^{-3}\,s^{-1}$.

existing linearization methods are used. Instead, the linearization form, i.e., Eq. (11a), obtained from the newly developed incremental secant linearization method is the same as that provided by the linearization methods for the elasto-plastic composites. Thus, the correspondent homogenization approaches established for the elasto-plastic composites are also suitable to consider the interaction among the constituent phases in the elasto-viscoplastic composites if the newly proposed incremental secant linearization method is adopted. It implies that the homogenization approaches for the elasto-plastic and elasto-viscoplastic composites would be unified with the help of newly developed incremental secant linearization method.

4. Conclusion

A new incremental secant linearization method is developed for the elasto-viscoplastic constitutive model by reasonably handling the unmatched time scales of elastic and viscoplastic deformations. And then this new linearization method is implemented into the M−T approach and SC one. Finally, the tensile deformations of elasto-viscoplastic microscopic heterogeneous materials (including the composites with different inclusion volume fractions, viscosities and hardening moduli, and the polycrystalline aggregates) under different loading conditions are predicted by the M−T and SC approaches based on the newly developed incremental secant linearization method. The predicted stress–strain curves are compared with that obtained by the FEM and FFT methods. Some key conclusions are obtained as:

(1) The elasto-viscoplastic constitutive model of each constituent is effectively linearized by the new incremental secant linearization method, and then the homogenization schemes based on the new linearization method can reasonably and accurately predict the overall tensile deformations of elasto-viscoplastic microscopic heterogeneous materials.

(2) Since the unmatched time scales between the elastic and viscoplastic deformations are effectively dealt with, the size of loading step has little effect on the predicted results of elasto-viscoplastic heterogeneous materials by the homogenization approaches based on the new linearization method, if the size of loading step is fine enough to capture the short-term and long-term viscoplastic behaviors.

(3) Since the linearized equation, i.e., Eq. (11a), obtained from the incremental secant linearization method has the same mathematical structure as that from the existing methods for the rate-independent elasto-plastic constitutive models, the MFH approaches for elasto-plastic and elasto-viscoplastic heterogeneous materials can be unified with the help of newly developed incremental secant linearization method.

It should be noted that the newly developed secant linearization method will be extended to the viscoelastic-viscoplastic heterogeneous materials in further work so that the linearization method of rate-dependent constitutive models can be unified further, although its effectiveness and accuracy are only verified for the elasto-viscoplastic microscopic heterogeneous materials in this work. Of course, there are still some shortcomings in our current work. For example, the new linearization method based MFH approach used here is unable to simulate the creep or relaxation of some composites. Thus, we are actively trying to deal with these shortcomings in future work.

CRediT authorship contribution statement

Wei Rao: Conceptualization, Data curation, Formal analysis, Funding acquisition, Investigation, Methodology, Supervision, Validation, Writing - original draft, Writing - review & editing. **Chao Yu:** Data curation, Supervision, Validation. **Juan Zhang:** Formal analysis, Funding acquisition, Supervision. **Guozheng Kang:** Formal analysis, Funding acquisition, Supervision, Writing - review & editing.

Declaration of Competing Interest

The authors declare that they have no known competing financial interests or personal relationships that could have appeared to influence the work reported in this paper.

Acknowledgement

Financial support from National Natural Science Foundation of China (Nos. 12002342; 11532010; 11572265) is appreciated.

Appendix A

From Eqs. (1c) and (1d), we can obtain that

$$\Delta\boldsymbol{\varepsilon}_{n+1}^{vp}=\dot{\boldsymbol{\varepsilon}}_{n+1}^{vp}\Delta t_{n+1}=\tilde{\boldsymbol{\varepsilon}}^{p'}(\boldsymbol{\sigma}_{n+1},\boldsymbol{V}_{n+1})\Delta t_{n+1}=\tilde{\boldsymbol{\varepsilon}}^{p'}(\boldsymbol{\sigma}_{n+1},\boldsymbol{V}_{n+1},\Delta t_{n+1}) \tag{A1}$$

$$\begin{aligned}\Delta\boldsymbol{V}_{n+1}&=\dot{\boldsymbol{V}}_{n+1}\Delta t_{n+1}=\tilde{\boldsymbol{V}}\left(\boldsymbol{\sigma}_{n+1},\dot{\boldsymbol{\varepsilon}}_{n+1}^{vp},\boldsymbol{V}_{n+1}\right)\Delta t_{n+1}\\&=\tilde{\boldsymbol{V}}'\left(\boldsymbol{\sigma}_{n+1},\dot{\boldsymbol{\varepsilon}}_{n+1}^{vp},\boldsymbol{V}_{n+1},\Delta t_{n+1}\right)\end{aligned} \tag{A2}$$

In a small increment step, it can be given as

$$\begin{aligned}\dot{\boldsymbol{\varepsilon}}_{n+1}^{vp}&\approx\frac{\Delta\boldsymbol{\varepsilon}_{n+1}^{vp}}{\Delta t_{n+1}}, & \boldsymbol{V}_{n+1}\\&=\boldsymbol{V}_n+\Delta\boldsymbol{V}_{n+1}, & \boldsymbol{\sigma}_{n+1}=\boldsymbol{\sigma}_n+\Delta\boldsymbol{\sigma}_{n+1}\end{aligned} \tag{A3}$$

Combining Eqs. (A2) and (A3), then

$$\begin{aligned}\Delta\boldsymbol{V}_{n+1}&=\tilde{\boldsymbol{V}}'\left(\boldsymbol{\sigma}_{n+1},\dot{\boldsymbol{\varepsilon}}_{n+1}^{vp},\boldsymbol{V}_{n+1},\Delta t_{n+1}\right)\\&=\tilde{\boldsymbol{V}}'\left(\Delta\boldsymbol{\sigma}_{n+1}+\boldsymbol{\sigma}_n,\frac{\Delta\boldsymbol{\varepsilon}_{n+1}^{vp}}{\Delta t_{n+1}},\boldsymbol{V}_n+\Delta\boldsymbol{V}_{n+1},\Delta t_{n+1}\right)\\&=\tilde{\boldsymbol{V}}''\left(\Delta\boldsymbol{\sigma}_{n+1},\boldsymbol{\sigma}_n,\Delta\boldsymbol{\varepsilon}_{n+1}^{vp},\boldsymbol{V}_n,\Delta\boldsymbol{V}_{n+1},\Delta t_{n+1}\right)\end{aligned} \tag{A4}$$

Eq. (A4) is an implicit function of $\Delta\boldsymbol{V}_{n+1}$. From this implicit function, we can give an explicit function of $\Delta\boldsymbol{V}_{n+1}$ as

$$\Delta\boldsymbol{V}_{n+1}=\tilde{\boldsymbol{V}}'''\left(\Delta\boldsymbol{\sigma}_{n+1},\boldsymbol{\sigma}_n,\Delta\boldsymbol{\varepsilon}_{n+1}^{vp},\boldsymbol{V}_n,\Delta t_{n+1}\right) \tag{A5}$$

Combining Eqs. (A1) and (A5), then

$$\begin{aligned}\Delta\boldsymbol{\varepsilon}_{n+1}^{vp}&=\tilde{\boldsymbol{\varepsilon}}^{p'}\left(\boldsymbol{\sigma}_{n+1},\boldsymbol{V}_{n+1},\Delta t_{n+1}\right)\\&=\tilde{\boldsymbol{\varepsilon}}^{p'}\left[\Delta\boldsymbol{\sigma}_{n+1}+\boldsymbol{\sigma}_n,\boldsymbol{V}_n+\Delta\boldsymbol{V}_{n+1},\Delta t_{n+1}\right]\\&=\tilde{\boldsymbol{\varepsilon}}^{p'}\left[\Delta\boldsymbol{\sigma}_{n+1}+\boldsymbol{\sigma}_n,\boldsymbol{V}_n+\tilde{\boldsymbol{V}}'''\left(\Delta\boldsymbol{\sigma}_{n+1},\boldsymbol{\sigma}_n,\Delta\boldsymbol{\varepsilon}_{n+1}^{vp},\boldsymbol{V}_n,\Delta t_{n+1}\right),\Delta t_{n+1}\right]\\&=\tilde{\boldsymbol{\varepsilon}}^{p''}\left(\Delta\boldsymbol{\sigma}_{n+1},\boldsymbol{\sigma}_n,\Delta\boldsymbol{\varepsilon}_{n+1}^{vp},\boldsymbol{V}_n,\Delta t_{n+1}\right)\end{aligned} \tag{A6}$$

Eq. (A6) is also an implicit function of $\Delta\boldsymbol{\varepsilon}_{n+1}^{vp}$. From this implicit function, we can give an explicit function of $\Delta\boldsymbol{\varepsilon}_{n+1}^{vp}$ as

$$\Delta\boldsymbol{\varepsilon}_{n+1}^{vp}=\tilde{\boldsymbol{\varepsilon}}^{p'''}\left(\Delta\boldsymbol{\sigma}_{n+1},\boldsymbol{\sigma}_n,\boldsymbol{V}_n,\Delta t_{n+1}\right) \tag{A7}$$

From Eqs. (1a) and (1c), it can be obtained that

$$\Delta\boldsymbol{\sigma}_{n+1}=\boldsymbol{C}:\left(\Delta\boldsymbol{\varepsilon}_{n+1}-\Delta\boldsymbol{\varepsilon}_{n+1}^{vp}\right) \tag{A8}$$

Substituting Eqs. (A7) into (A8), it yields

$$\begin{aligned}\Delta\boldsymbol{\sigma}_{n+1}&=\boldsymbol{C}:\left(\Delta\boldsymbol{\varepsilon}_{n+1}-\Delta\boldsymbol{\varepsilon}_{n+1}^{vp}\right)\\&=\boldsymbol{C}:\left[\Delta\boldsymbol{\varepsilon}_{n+1}-\tilde{\boldsymbol{\varepsilon}}^{p'''}\left(\Delta\boldsymbol{\sigma}_{n+1},\boldsymbol{\sigma}_n,\boldsymbol{V}_n,\Delta t_{n+1}\right)\right]\end{aligned} \tag{A9}$$

Since $\boldsymbol{C}$ is constant, we can think that $\Delta\boldsymbol{\sigma}_{n+1}$ is a function of $\Delta\boldsymbol{\varepsilon}_{n+1}$, $\Delta\boldsymbol{\sigma}_{n+1}$, $\boldsymbol{\sigma}_n$, $\boldsymbol{V}_n$ and Δt_{n+1}. Thus, a function can be given as

$$\Delta\boldsymbol{\sigma}_{n+1}=\boldsymbol{\sigma}'(\Delta\boldsymbol{\varepsilon}_{n+1},\Delta\boldsymbol{\sigma}_{n+1},\boldsymbol{\sigma}_n,\boldsymbol{V}_n,\Delta t_{n+1}\ ) \tag{10}$$

Eq. (A10) is an implicit function of $\Delta\boldsymbol{\sigma}_{n+1}$. If we transform it into an explicit form, Eq. (2) can be obtained.

Appendix B

B1 incremental secant linearization-based Mori-Tanaka's approach

According to the newly proposed incremental secant linearization method, the linear relationships between the volume averaged stress increment and volume averaged strain one in the matrix and inclusion phases are expressed as

$$\langle\Delta\boldsymbol{\sigma}_{n+1}\rangle_M=\left(\boldsymbol{C}_{n+1}^{sec}\right)_M:\langle\Delta\boldsymbol{\varepsilon}_{n+1}\rangle_M. \tag{1a}$$

$$\langle\Delta\boldsymbol{\sigma}_{n+1}\rangle_I=\left(\boldsymbol{C}_{n+1}^{sec}\right)_I:\langle\Delta\boldsymbol{\varepsilon}_{n+1}\rangle_I. \tag{1b}$$

where $\langle\Delta\boldsymbol{\sigma}_{n+1}\rangle_M$ and $\langle\Delta\boldsymbol{\sigma}_{n+1}\rangle_I$ are the volume averaged stress increments, $\langle\Delta\boldsymbol{\varepsilon}_{n+1}\rangle_M$ and $\langle\Delta\boldsymbol{\varepsilon}_{n+1}\rangle_I$ are the volume averaged strain increments, and $\left(\boldsymbol{C}_{n+1}^{sec}\right)_M$ and $\left(\boldsymbol{C}_{n+1}^{sec}\right)_I$ are the incremental secant modulus tensors of matrix and inclusion, respectively. Hereafter, $(\cdot)_M$and $(\cdot)_I$ denote that the $(\cdot)$ belong to the matrix and inclusion, respectively.

From the Eshelby's theory, a heterogeneous problem can be equivalent to a homogeneous inclusion one. Thus,

$$\langle\Delta\boldsymbol{\sigma}_{n+1}\rangle_I=\left(\boldsymbol{C}_{n+1}^{sec}\right)_I:\langle\Delta\boldsymbol{\varepsilon}_{n+1}\rangle_I=\left(\boldsymbol{C}_{n+1}^{sec}\right)_M:\left(\langle\Delta\boldsymbol{\varepsilon}_{n+1}\rangle_I-\Delta\boldsymbol{\varepsilon}_{n+1}^{*}\right) \tag{B2}$$

where $\Delta\boldsymbol{\varepsilon}_{n+1}^{*}$ is an increment of eigenstrain tensor. Referring to Rao et al. [41,42], a relationship between the increments of eigenstrain and disturbance strain is written as:

$$\langle\Delta\boldsymbol{\varepsilon}_{n+1}\rangle_I-\langle\Delta\boldsymbol{\varepsilon}_{n+1}\rangle_M=\boldsymbol{S}_{n+1}:\Delta\boldsymbol{\varepsilon}_{n+1}^{*} \tag{B3}$$

Here, $\boldsymbol{S}_{n+1}$ is the Eshelby's tensor [43].

Combining Eqs. (B2) with (B3), it yields

$$\begin{aligned}\langle\Delta\boldsymbol{\varepsilon}_{n+1}\rangle_M=&\left\{\boldsymbol{S}_{n+1}:\left[\left(\boldsymbol{C}_{n+1}^{sec}\right)_M\right]^{-1}:\left[\left(\boldsymbol{C}_{n+1}^{sec}\right)_I-\left(\boldsymbol{C}_{n+1}^{sec}\right)_M\right]+\boldsymbol{I}\right\}\\&:\langle\Delta\boldsymbol{\varepsilon}_{n+1}\rangle_I\end{aligned} \tag{B4}$$

Let

$$\boldsymbol{B}_{n+1}=\boldsymbol{S}_{n+1}:\left[\left(\boldsymbol{C}_{n+1}^{sec}\right)_M\right]^{-1}:\left[\left(\boldsymbol{C}_{n+1}^{sec}\right)_I-\left(\boldsymbol{C}_{n+1}^{sec}\right)_M\right]+\boldsymbol{I} \tag{B5}$$

Then, Eq. (B4) can be rewritten as

$$\langle\Delta\boldsymbol{\varepsilon}_{n+1}\rangle_M=\boldsymbol{B}_{n+1}\ :\langle\Delta\boldsymbol{\varepsilon}_{n+1}\rangle_I \tag{B6}$$

The relationship between the overall strain increment and local volume averaged strain one can be given as

$$\Delta\bar{\boldsymbol{\varepsilon}}_{n+1}=(1-f)\langle\Delta\boldsymbol{\varepsilon}_{n+1}\rangle_M+f\langle\Delta\boldsymbol{\varepsilon}_{n+1}\rangle_I \tag{B7}$$

Here, f is the volume fraction of inclusion phase.

Combining Eqs. (B6) with (B7), it yields

$$\langle\Delta\boldsymbol{\varepsilon}_{n+1}\rangle_I=\left[(1-f)\boldsymbol{B}_{n+1}+f\boldsymbol{I}\right]^{-1}:\Delta\bar{\boldsymbol{\varepsilon}}_{n+1} \tag{B8}$$

Combining Eqs. (B6) with (B8), it yields

$$\langle \Delta\boldsymbol{\varepsilon}_{n+1}\rangle_M = \boldsymbol{B}_{n+1} : [(1-f)\boldsymbol{B}_{n+1} + f\boldsymbol{I}]^{-1} : \Delta\bar{\boldsymbol{\varepsilon}}_{n+1} \tag{B9}$$

Similarly, a relationship between the overall and local volume averaged stress increments can be given as

$$\Delta\bar{\boldsymbol{\sigma}}_{n+1} = (1-f)\langle \Delta\boldsymbol{\sigma}_{n+1}\rangle_M + f\langle \Delta\boldsymbol{\sigma}_{n+1}\rangle_I \tag{B10}$$

Substituting Eqs. (B1a), (B1b), (B8) and (B9) into Eq. (B10), it yields

$$\Delta\bar{\boldsymbol{\sigma}}_{n+1} = \bar{\boldsymbol{C}}^{sec}_{n+1} : \Delta\bar{\boldsymbol{\varepsilon}}_{n+1} \tag{11a}$$

$$\bar{\boldsymbol{C}}^{sec}_{n+1} = (1-f)\left[\boldsymbol{C}^{sec}_{n+1}\right]_M : \boldsymbol{B}_{n+1} : [(1-f)\boldsymbol{B}_{n+1} + f\boldsymbol{I}]^{-1} + f\left[\boldsymbol{C}^{sec}_{n+1}\right]_I : [(1-f)\boldsymbol{B}_{n+1} + f\boldsymbol{I}]^{-1} \tag{B11b}$$

where $\bar{\boldsymbol{C}}^{sec}_{n+1}$ is the equivalent incremental secant modulus tensor of the composites.

3.2. Incremental secant linearization-based self-consistent approach

After linearization, the constitutive equations can be rewritten as:

$$\langle \Delta\boldsymbol{\sigma}_{n+1}\rangle_I = \left(\boldsymbol{C}^{sec}_{n+1}\right)_I : \langle \Delta\boldsymbol{\varepsilon}_{n+1}\rangle_I \tag{B12}$$

The macroscopic overall constitutive equation of heterogeneous material can also be written as the following affine form:

$$\Delta\bar{\boldsymbol{\sigma}}_{n+1} = \bar{\boldsymbol{C}}^{sec}_{n+1} : \Delta\bar{\boldsymbol{\varepsilon}}_{n+1} \tag{B13}$$

where $\Delta\bar{\boldsymbol{\varepsilon}}_{n+1}$ and $\Delta\bar{\boldsymbol{\sigma}}_{n+1}$ are the macroscopic overall strain and stress increments, respectively, and $\bar{\boldsymbol{C}}^{sec}_{n+1}$ is the effective incremental secant modulus.

Different from the M−T one, the SC homogenization approach assumes that the inclusion is embedded into an equivalent medium with the same overall response as that of microscopic heterogeneous material. Thus, according to the Eshelby's equivalent inclusion theory, the effective modulus tensor of the inclusion can be replaced by that of homogeneous equivalent medium once an artificial eigenstrain increment is introduced. Then, a similar constitutive equation between the local phase and overall polycrystalline aggregates can be obtained as the following equivalent form:

$$\langle \Delta\boldsymbol{\sigma}_{n+1}\rangle_I = \left(\boldsymbol{C}^{sec}_{n+1}\right)_I : \langle \Delta\boldsymbol{\varepsilon}_{n+1}\rangle_I = \bar{\boldsymbol{C}}^{sec}_{n+1} : \left(\langle \Delta\boldsymbol{\varepsilon}_{n+1}\rangle - \Delta\bar{\boldsymbol{\varepsilon}}^{*}\right) \tag{B14}$$

where $\Delta\bar{\boldsymbol{\varepsilon}}^{*}$ is the eigenstrain increment.

Based on the Eshelby's inclusion theory and the hypothesis of SC homogenization approach, the volume averages of strain increments in the matrix and equivalent medium and the eigenstrain increment can be linked by the Eshelby's tensor $\boldsymbol{S}$, i.e.,

$$\langle \Delta\boldsymbol{\varepsilon}_{n+1}\rangle_I - \Delta\bar{\boldsymbol{\varepsilon}}_{n+1} = \boldsymbol{S} : \Delta\boldsymbol{\varepsilon}^{*} \tag{B15}$$

Substituting Eq. (B15) into Eq. (B14), it yields

$$\langle \Delta\boldsymbol{\varepsilon}_{n+1}\rangle_I = \left[\boldsymbol{S} : \left(\bar{\boldsymbol{C}}^{sec}_{n+1}\right)^{-1} : \left(\boldsymbol{C}^{sec}_{n+1}\right)_I - (\boldsymbol{S}-\boldsymbol{I})\right]^{-1} : \Delta\bar{\boldsymbol{\varepsilon}}_{n+1} \tag{B16}$$

Let

$$\boldsymbol{B}_I = \left[\boldsymbol{S} : \left(\bar{\boldsymbol{C}}^{sec}_{n+1}\right)^{-1} : \left(\boldsymbol{C}^{sec}_{n+1}\right)_I - (\boldsymbol{S}-\boldsymbol{I})\right]^{-1} \tag{B17}$$

Then, Eq. (B16) can be rewritten as

$$\langle \Delta\boldsymbol{\varepsilon}_{n+1}\rangle_I = \boldsymbol{B}_I : \Delta\bar{\boldsymbol{\varepsilon}}_{n+1} \tag{B18}$$

Following the rules of mixture, the relationship between the overall stress increment of heterogeneous material and the volume averages of the stress increments in the local phases can be shown as

$$\Delta\bar{\boldsymbol{\sigma}}_{n+1} = \sum_{I=1}^{n} f_I \langle \Delta\boldsymbol{\sigma}_{n+1}\rangle_I \tag{B19}$$

Substituting Eqs. (B12), (B18) and (B19) into Eq. (B19), it yields

$$\Delta\bar{\boldsymbol{\sigma}}_{n+1} = \sum_{I=1}^{n} f_I \left(\boldsymbol{C}^{sec}_{n+1}\right)_I : \boldsymbol{B}_I : \Delta\bar{\boldsymbol{\varepsilon}}_{n+1} \tag{B20}$$

And the effective incremental secant modulus tensor of polycrystalline aggregates is expressed as

$$\bar{\boldsymbol{C}}^{sec}_{n+1} = \sum_{I=1}^{n} f_I \left(\boldsymbol{C}^{sec}_{n+1}\right)_I : \boldsymbol{B}_I \tag{B21}$$

Appendix C

In this subsection, a unified elasto-viscoplastic constitutive model used in Section 4.1 is given. Furthermore, to apply it into the M−T approach, its linearization is also deduced by using the incremental secant linearization method.

Appendix C. 1 main equations of elasto-viscoplasticity constitutive model

In a unified elasto-viscoplastic constitutive model, the strain tensor $\boldsymbol{\varepsilon}$ can be divided into an elastic part $\boldsymbol{\varepsilon}^{e}$ and viscoplastic one $\boldsymbol{\varepsilon}^{vp}$, then

$$\boldsymbol{\varepsilon} = \boldsymbol{\varepsilon}^{e} + \boldsymbol{\varepsilon}^{vp} \tag{C1}$$

The Hooke's law is expressed as

$$\boldsymbol{\sigma} = \boldsymbol{C} : \boldsymbol{\varepsilon}^{e} \tag{C2}$$

The von Mises's equivalent stress σ^{eq} can be written as

$$\sigma^{eq} = \sqrt{\frac{3}{2}(\boldsymbol{s}-\boldsymbol{\alpha}) : (\boldsymbol{s}-\boldsymbol{\alpha})} \tag{C3}$$

where $\boldsymbol{s} = \mathrm{dev}(\boldsymbol{\sigma})$ denotes a deviatoric stress tensor, and $\boldsymbol{\alpha}$ denotes a back stress tensor.

The viscoplastic strain rate $\dot{\boldsymbol{\varepsilon}}^{vp}$ is

$$\dot{\boldsymbol{\varepsilon}}^{vp} = \sqrt{\frac{3}{2}}\dot{\gamma}\boldsymbol{N} \tag{C4}$$

where $\dot{\gamma}$ is the viscoplastic flow rate, and $\boldsymbol{N}$ denotes the viscoplastic flow direction.

The viscoplastic flow rate $\dot{\gamma}$ is taken as

$$\dot{\gamma} = \dot{\gamma}_0 \left\langle \frac{f}{R} \right\rangle^{m} \tag{C5}$$

where $\dot{\gamma}_0$ is the referential viscoplastic multiplier; $f = \sigma^{eq} - R$ is the driving force; R denotes the viscoplastic flow resistance, m is a power-law exponent. is Macauley's bracket, i.e., as $x < 0$, $\langle x\rangle = 0$; as $x \geqslant 0$, $\langle x\rangle = x$.

The viscoplastic flow direction $\boldsymbol{N}$ is

$$\boldsymbol{N} = \frac{\boldsymbol{s}-\boldsymbol{\alpha}}{\| \boldsymbol{s}-\boldsymbol{\alpha} \|} \tag{C6}$$

The back stress $\boldsymbol{\alpha}$ is simply taken as

$$\dot{\boldsymbol{\alpha}} = \frac{2}{3}h\dot{\boldsymbol{\varepsilon}}^{p} - \xi\boldsymbol{\alpha}\dot{\gamma} \tag{C7}$$

Here, h denotes a material parameter, ξ denotes a dynamic recovery coefficient.

The resistance R can be expressed as

$$R = \sigma_0 + K\gamma^{a} \tag{C8}$$

where, σ_0 denotes the initial yielding stress, K and a are two parameters.

Appendix C. 2 deducing the incremental secant modulus tensor

Consider the time interval of Δt_{n+1}, and assume that the solutions at the time t_n are known, and a total strain increment $\Delta\boldsymbol{\varepsilon}_{n+1}$ and time increment Δt_{n+1} at this time interval are given, respectively. The elasto-viscoplastic constitutive equations are discretized first. Such discrete equations are

$$\Delta\boldsymbol{\sigma}_{n+1} = \boldsymbol{C} : \left(\Delta\boldsymbol{\varepsilon}_{n+1} - \Delta\boldsymbol{\varepsilon}^{p}_{n+1}\right) \tag{C9a}$$

$$\Delta\boldsymbol{\varepsilon}^{vp}_{n+1} = \sqrt{\frac{3}{2}}\Delta\gamma_{n+1}\boldsymbol{N}_{n+1} \tag{C9b}$$

$$\Delta\boldsymbol{\alpha}_{n+1} = \frac{2}{3}h\Delta\boldsymbol{\varepsilon}^{vp}_{n+1} - \xi\boldsymbol{\alpha}_{n+1}\Delta\gamma_{n+1} \tag{C9c}$$

$$\sigma^{eq}_{n+1} = \sqrt{\frac{3}{2}}\| \boldsymbol{s}_{n+1} - \boldsymbol{\alpha}_{n+1} \| \tag{C9d}$$

$$\Delta\gamma_{n+1} = \dot{\gamma}_0\left\langle\frac{\sigma^{eq}_{n+1} - R_{n+1}}{R_{n+1}}\right\rangle^{m}\Delta t_{n+1} \tag{C9e}$$

$$\boldsymbol{N}_{n+1} = \frac{\boldsymbol{s}_{n+1} - \boldsymbol{\alpha}_{n+1}}{\| \boldsymbol{s}_{n+1} - \boldsymbol{\alpha}_{n+1} \|} \tag{C9f}$$

$$R_{n+1} = \sigma_0 + K\gamma^{a}_{n+1} \tag{C9g}$$

Differentiating all items in Eq. (C9e), it yields

$$\begin{aligned}
\mathrm{d}\Delta\gamma_{n+1} &= \mathrm{d}\left[\dot{\gamma}_0\left\langle\tfrac{f_{n+1}}{R_{n+1}}\right\rangle^{m}\Delta t_{n+1}\right] \\
&= m\dot{\gamma}_0\left(\tfrac{f_{n+1}}{R_{n+1}}\right)^{m}\Delta t_{n+1}\left(\tfrac{\mathrm{d}f_{n+1}}{f_{n+1}} - \tfrac{\mathrm{d}R_{n+1}}{R_{n+1}}\right) + \dot{\gamma}_0\left(\tfrac{f_{n+1}}{R_{n+1}}\right)^{m}\mathrm{d}\Delta t_{n+1} \\
&= m\Delta\gamma_{n+1}\left(\tfrac{\mathrm{d}\sigma^{eq}_{n+1}}{f_{n+1}} - \tfrac{\mathrm{d}R_{n+1}}{f_{n+1}} - \tfrac{\mathrm{d}R_{n+1}}{R_{n+1}}\right) + \tfrac{\Delta\gamma_{n+1}}{\Delta t_{n+1}}\mathrm{d}\Delta t_{n+1} \\
&= m\Delta\gamma_{n+1}\left(\tfrac{\mathrm{d}\sigma^{eq}_{n+1}}{f_{n+1}} - \tfrac{\mathrm{d}R_{n+1}}{f_{n+1}} - \tfrac{aK\gamma^{a-1}_{n+1}\mathrm{d}\gamma_{n+1}}{R_{n+1}}\right) + \tfrac{\Delta\gamma_{n+1}}{\Delta t_{n+1}}\mathrm{d}\Delta t_{n+1} \\
&= m\Delta\gamma_{n+1}\left(\tfrac{\mathrm{d}\sigma^{eq}_{n+1}}{f_{n+1}} - \tfrac{\mathrm{d}R_{n+1}}{f_{n+1}} - \tfrac{aK\gamma^{a-1}_{n+1}\left(\mathrm{d}\gamma_n + \mathrm{d}\Delta\gamma_{n+1}\right)}{R_{n+1}}\right) + \tfrac{\Delta\gamma_{n+1}}{\Delta t_{n+1}}\mathrm{d}\Delta t_{n+1} \\
&= m\Delta\gamma_{n+1}\left(\tfrac{\mathrm{d}\sigma^{eq}_{n+1}}{f_{n+1}} - \tfrac{\mathrm{d}R_{n+1}}{f_{n+1}} - \tfrac{aK\gamma^{a-1}_{n+1}\mathrm{d}\Delta\gamma_{n+1}}{R_{n+1}}\right) + \tfrac{\Delta\gamma_{n+1}}{\Delta t_{n+1}}\mathrm{d}\Delta t_{n+1} \\
&= A\left[\sqrt{\tfrac{3}{2}}m\Delta\gamma_{n+1}\tfrac{\boldsymbol{N}_{n+1}:\mathrm{d}(\boldsymbol{s}_{n+1}-\boldsymbol{\alpha}_{n+1})}{f_{n+1}} + \tfrac{\Delta\gamma_{n+1}}{\Delta t_{n+1}}\mathrm{d}\Delta t_{n+1}\right]
\end{aligned} \tag{C10}$$

where, $A = \left[1 + m\Delta\gamma_{n+1}Ka\gamma^{a-1}_{n+1}\left(\frac{1}{f_{n+1}} + \frac{1}{R_{n+1}}\right)\right]^{-1}$. It should be noted that $\mathrm{d}\gamma_n = 0$ since γ_n is a constant at the time increment Δt_{n+1}. In fact, the solutions of $(\cdot)$ at the time t_n are known, which implies that $\mathrm{d}(\cdot)_n = 0$.

Differentiating all items in Eq. (C9f), it can be obtained that

$$\begin{aligned}
\mathrm{d}\boldsymbol{N}_{n+1} &= \mathrm{d}\left(\tfrac{\boldsymbol{s}_{n+1}-\boldsymbol{\alpha}_{n+1}}{\|\boldsymbol{s}_{n+1}-\boldsymbol{\alpha}_{n+1}\|}\right) \\
&= \tfrac{\boldsymbol{I}-\boldsymbol{N}_{n+1}\otimes\boldsymbol{N}_{n+1}}{\|\boldsymbol{s}_{n+1}-\boldsymbol{\alpha}_{n+1}\|} : \mathrm{d}\left(\boldsymbol{s}_{n+1} - \boldsymbol{\alpha}_{n+1}\right)
\end{aligned} \tag{C11}$$

Differentiating all items in Eq. (C9c), it yields

$$\begin{aligned}
\mathrm{d}\Delta\boldsymbol{\alpha}_{n+1} &= \mathrm{d}\left(\tfrac{2}{3}h\Delta\boldsymbol{\varepsilon}^{p}_{n+1} - \xi\boldsymbol{\alpha}_{n+1}\Delta\gamma_{n+1}\right) \\
&= \tfrac{2}{3}h\mathrm{d}\Delta\boldsymbol{\varepsilon}^{p}_{n+1} - \xi\mathrm{d}\boldsymbol{\alpha}_{n+1}\Delta\gamma_{n+1} - \xi\boldsymbol{\alpha}_{n+1}\mathrm{d}\Delta\gamma_{n+1}
\end{aligned} \tag{C12}$$

Combining Eq. (C10) and Eq. (C12), it yields

$$\mathrm{d}\Delta\boldsymbol{\alpha}_{n+1} = \boldsymbol{H}_{1} : \left[\tfrac{2}{3}h\mathrm{d}\Delta\boldsymbol{\varepsilon}^{p}_{n+1} - \xi A\left(\sqrt{\tfrac{3}{2}}m\Delta\gamma_{n+1}\tfrac{\boldsymbol{\alpha}_{n+1}\otimes\boldsymbol{N}_{n+1}:\mathrm{d}\boldsymbol{s}_{n+1}}{f_{n+1}} + \tfrac{\Delta\gamma_{n+1}}{\Delta t_{n+1}}\boldsymbol{\alpha}_{n+1}\mathrm{d}\Delta t_{n+1}\right)\right] \tag{C13}$$

where

$$\boldsymbol{H}_{1} = \left[(1 + \xi\Delta\gamma_{n+1})\boldsymbol{I} - \sqrt{\frac{3}{2}}m\Delta\gamma_{n+1}\xi A\frac{\boldsymbol{\alpha}_{n+1}\otimes\boldsymbol{N}_{n+1}}{f_{n+1}}\right]^{-1} \tag{C14}$$

Differentiating all items in Eq. (C9b), it gives

$$\begin{aligned}
\mathrm{d}\Delta\boldsymbol{\varepsilon}^{vp}_{n+1} &= \mathrm{d}\left(\sqrt{\tfrac{3}{2}}\Delta\gamma_{n+1}\boldsymbol{N}_{n+1}\right) \\
&= \sqrt{\tfrac{3}{2}}\mathrm{d}\Delta\gamma_{n+1}\boldsymbol{N}_{n+1} + \sqrt{\tfrac{3}{2}}\Delta\gamma_{n+1}\mathrm{d}\boldsymbol{N}_{n+1}.
\end{aligned} \tag{15}$$

Substituting Eqs. (C10), (C11) and (C12) into Eq. (C15), it gives

$$\begin{aligned}
\mathrm{d}\Delta\boldsymbol{\varepsilon}^{vp}_{n+1} &= \left[\boldsymbol{I} + \tfrac{2}{3}h\boldsymbol{H}_2 : \boldsymbol{H}_{1}\right]^{-1} : \left[\boldsymbol{H}_3 : \mathrm{d}\boldsymbol{\sigma}_{n+1} + \left(\xi\boldsymbol{H}_2 : \boldsymbol{H}_{1} : \boldsymbol{\alpha}_{n+1} + \sqrt{\tfrac{3}{2}}\boldsymbol{N}_{n+1}\right)\right. \\
&\quad \left. A\tfrac{\Delta\gamma_{n+1}}{\Delta t_{n+1}}\mathrm{d}\Delta t_{n+1}\right]
\end{aligned}$$

where

$$\boldsymbol{H}_2 = \frac{3}{2}Am\Delta\gamma_{n+1}\frac{\boldsymbol{N}_{n+1}\otimes\boldsymbol{N}_{n+1}}{f_{n+1}} + \sqrt{\frac{3}{2}}\Delta\gamma_{n+1} \times \frac{\boldsymbol{I}_d - \boldsymbol{N}_{n+1}\otimes\boldsymbol{N}_{n+1}}{\| \boldsymbol{s}_{n+1} - \boldsymbol{\alpha}_{n+1} \|} \tag{C17a}$$

$$\boldsymbol{H}_{3} = \left(\boldsymbol{H}_2 + \sqrt{\frac{3}{2}}m\Delta\gamma_{n+1}\xi A\frac{\boldsymbol{H}_2 : \boldsymbol{H}_{1} : \boldsymbol{\alpha}_{n+1}\otimes\boldsymbol{N}_{n+1}}{f_{n+1}}\right) \tag{C17b}$$

Differentiating all items in Eq. (C9a), it gives

$$\begin{aligned}
\mathrm{d}\Delta\boldsymbol{\sigma}_{n+1} &= \boldsymbol{C} : \left(\mathrm{d}\Delta\boldsymbol{\varepsilon}_{n+1} - \mathrm{d}\Delta\boldsymbol{\varepsilon}^{vp}_{n+1}\right) \\
&= \left[\boldsymbol{I} + 2\mu\left(\boldsymbol{I} + \tfrac{2}{3}h\boldsymbol{H}_2 : \boldsymbol{H}_{1}\right)^{-1} : \boldsymbol{H}_3\right]^{-1} : \left[\boldsymbol{C} : \mathrm{d}\Delta\boldsymbol{\varepsilon}_{n+1} - 2\mu\right. \\
&\quad \left.\left(\boldsymbol{I} + \tfrac{2}{3}h\boldsymbol{H}_2 : \boldsymbol{H}_{1}\right)^{-1} : \left(\xi\boldsymbol{H}_2 : \boldsymbol{H}_{1} : \boldsymbol{\alpha}_{n+1} + \sqrt{\tfrac{3}{2}}\boldsymbol{N}_{n+1}\right)A\tfrac{\Delta\gamma_{n+1}}{\Delta t_{n+1}}\mathrm{d}\Delta t_{n+1}\right]
\end{aligned} \tag{C18}$$

Let

$$\boldsymbol{H}_4 = \left[\boldsymbol{I} + 2\mu\left(\boldsymbol{I} + \frac{2}{3}h\boldsymbol{H}_2 : \boldsymbol{H}_{1}\right)^{-1} : \boldsymbol{H}_3\right]^{-1} \tag{C19a}$$

$$\boldsymbol{H}_5 = \mathrm{A}\boldsymbol{H}_4 : \left(\boldsymbol{I} + \frac{2}{3}h\boldsymbol{H}_2 : \boldsymbol{H}_{1}\right)^{-1} : \left(\sqrt{\frac{2}{3}}\xi\boldsymbol{H}_2 : \boldsymbol{H}_{1} : \boldsymbol{\alpha}_{n+1} + \boldsymbol{N}_{n+1}\right)\otimes\boldsymbol{N}_{n+1} \tag{C19b}$$

Then, Eq. (C18) is rewritten as

$$\mathrm{d}\Delta\boldsymbol{\sigma}_{n+1} = \boldsymbol{H}_4 : \boldsymbol{C} : \mathrm{d}\Delta\boldsymbol{\varepsilon}_{n+1} - \boldsymbol{H}_5 : 2\mu\sqrt{\frac{3}{2}}\frac{\Delta\gamma_{n+1}}{\Delta t_{n+1}}\boldsymbol{N}_{n+1}\mathrm{d}\Delta t_{n+1} \tag{C20}$$

Thus, it can be obtained from Eq. (C20) that

$$\frac{\partial\Delta\boldsymbol{\sigma}_{n+1}}{\partial\Delta\boldsymbol{\varepsilon}_{n+1}} = \boldsymbol{H}_4 : \boldsymbol{C} \tag{C21a}$$

$$\frac{\partial\Delta\boldsymbol{\sigma}_{n+1}}{\partial\Delta t_{n+1}} = -\boldsymbol{H}_5 : 2\mu\sqrt{\frac{3}{2}}\frac{\Delta\gamma_{n+1}}{\Delta t_{n+1}}\boldsymbol{N}_{n+1} \tag{C21b}$$

Substituting Eqs. (C21a) and (C21b) into Eq. (6), it yields

$$\Delta\boldsymbol{\sigma}_{n+1} \approx \boldsymbol{H}_4 : \boldsymbol{C} : \Delta\boldsymbol{\varepsilon}_{n+1} - \boldsymbol{H}_5 : 2\mu\sqrt{\frac{3}{2}}\frac{\Delta\gamma_{n+1}}{\Delta t_{n+1}}\boldsymbol{N}_{n+1}\Delta t_{n+1} \tag{C22}$$

Combining Eqs. (C9a) and (C21), it gives

$$\Delta\boldsymbol{\sigma}_{n+1} \approx (\boldsymbol{I} - \boldsymbol{H}_5)^{-1} : (\boldsymbol{H}_4 - \boldsymbol{H}_5) : \boldsymbol{C} : \Delta\boldsymbol{\varepsilon}_{n+1} \tag{C23}$$

Then, the incremental secant modulus tensor can be expressed as

$$\boldsymbol{C}^{sec}_{n+1} = (\boldsymbol{I} - \boldsymbol{H}_5)^{-1} : (\boldsymbol{H}_4 - \boldsymbol{H}_5) : \boldsymbol{C} \tag{C24}$$

Appendix D

In this subsection, some constitutive models used in Sections 4.2 and 4.3 are provided. Since the forms of these constitutive models are similar to that of the model listed in Appendix D1, the increment secant modulus tensors for such constitutive models listed in this subsection have a similar derivation process to that listed in Appendix D2.

Thus, we don't give the derivation process for their increment secant modulus tensors here.

Here, the main equations for the constitutive model with no plastic hardening are provided as

$$\boldsymbol{\varepsilon} = \boldsymbol{\varepsilon}^{\mathrm{e}} + \boldsymbol{\varepsilon}^{\mathrm{vp}} \tag{D1}$$

$$\boldsymbol{\sigma} = \boldsymbol{C} : \boldsymbol{\varepsilon}^{\mathrm{e}} \tag{D2}$$

$$\dot{\boldsymbol{\varepsilon}}^{\mathrm{vp}} = \sqrt{\frac{3}{2}}\dot{\gamma}\boldsymbol{N} \tag{D3}$$

$$\sigma^{\mathrm{eq}} = \sqrt{\frac{3}{2}\mathrm{dev}(\boldsymbol{s}) : \mathrm{dev}(\boldsymbol{s})} \tag{D4}$$

$$\dot{\gamma} = \dot{\gamma}_0 \left(\frac{\sigma^{\mathrm{eq}}}{\sigma_y}\right)^m \tag{D5}$$

$$\boldsymbol{N}_{\mathrm{n}+1} = \frac{\mathrm{dev}(\boldsymbol{s})}{\| \mathrm{dev}(\boldsymbol{s}) \|} \tag{D6}$$

where $\boldsymbol{C}$ is the elasticity tensor; $\dot{\gamma}_0$ is the referential viscoplastic multiplier; m is a power-law exponent; σ_y is the initial yielding stress; n is the hardening exponent.

Appendix E

In this subsection, the main equations of a constitutive model for a single crystal are provided, and the derivation process for its increment secant modulus tensor is also given.

Appendix E. 1 the main equations for the constitutive model of single crystal

In a unified elasto-viscoplastic constitutive model of single crystal, its strain tensor $\boldsymbol{\varepsilon}$ can be divided into an elastic part $\boldsymbol{\varepsilon}^{\mathrm{e}}$ and viscoplastic one $\boldsymbol{\varepsilon}^{\mathrm{vp}}$, then

$$\boldsymbol{\varepsilon} = \boldsymbol{\varepsilon}^{\mathrm{e}} + \boldsymbol{\varepsilon}^{\mathrm{vp}} \tag{E1}$$

The Hooke's law is expressed as

$$\boldsymbol{\sigma} = \boldsymbol{C} : \boldsymbol{\varepsilon}^{\mathrm{e}} \tag{E2}$$

where $\boldsymbol{C}$ is the elasticity tensor of single crystal.

The viscoplastic strain rate $\dot{\boldsymbol{\varepsilon}}^{\mathrm{vp}}$ can be expressed as

$$\dot{\boldsymbol{\varepsilon}}^{vp} = \sum_{s=1}^{N} \frac{1}{2}\dot{\gamma}^s(\boldsymbol{m}^s \otimes \boldsymbol{n}^s + \boldsymbol{n}^s \otimes \boldsymbol{m}^s) \tag{E3}$$

where $\dot{\gamma}^s$ is the viscoplastic shear strain rate for the slip system s. $\boldsymbol{m}^s$ and $\boldsymbol{n}^s$ are the direction of slip plane and the slip direction in the slip system s, respectively.

The evolution equation of viscoplastic shear strain rate can be given as

$$\dot{\gamma}^s = \left(\frac{\langle|\tau^s - x^s| - r^s\rangle}{k}\right)^m \mathrm{sign}(\tau^s - x^s) \tag{E4}$$

where x^s and r^s are the shear back stress and isotropic deformation resistance, respectively; k is a viscosity parameter, m is a strain rate sensitivity parameter; $\mathrm{sign}(\cdot)$ is a sign function, τ^s is the driving force for viscoplastic slip (i.e., the resolved shear stress in the slip system s), and its evolution is given as

$$\tau^s = \boldsymbol{\sigma} : (\boldsymbol{m}^s \otimes \boldsymbol{n}^s) \tag{E5}$$

The kinematic hardening rule representing the evolution of shear back stress can be expressed as

$$x^s = Ay^s\dot{y}^s = \dot{\gamma}^s - Dy^s|\dot{\gamma}^s| \tag{E6}$$

where A and D are two kinematic hardening parameters.

The evolution equation of isotropic deformation resistance can be given as

$$r^s = r_0 + \sum_{t=1}^{N} QH^{st}q^t\,\dot{q}^t = (1 - Bq^t)|\dot{\gamma}^t| \tag{E7}$$

where Q and B are two isotropic hardening parameters; H is the parameter matrix characterizing the interaction between different slip systems; r_0 is the initial critical resolved shear stress for the dislocation slipping in each slip system, which is assumed to be the same for each slip system here.

Appendix E. 2 deducing the incremental secant modulus tensor

Consider the time interval of $\Delta t_{\mathrm{n}+1}$, and assume that the solutions at the time t_{n} are known, and a total strain increment $\Delta\boldsymbol{\varepsilon}_{\mathrm{n}+1}$ and time increment $\Delta t_{\mathrm{n}+1}$ at this time interval are given, respectively. The elasto-viscoplastic constitutive equations of single crystal are discretized first. The discrete equations are

$$\Delta\boldsymbol{\sigma}_{\mathrm{n}+1} = \boldsymbol{C} : \left(\Delta\boldsymbol{\varepsilon}_{\mathrm{n}+1} - \Delta\boldsymbol{\varepsilon}^{\mathrm{p}}_{\mathrm{n}+1}\right) \tag{E8a}$$

$$\Delta\boldsymbol{\varepsilon}^{vp}_{n+1} = \sum_{s=1}^{N} \frac{1}{2}\Delta\gamma^s_{n+1}(\boldsymbol{m}^s \otimes \boldsymbol{n}^s + \boldsymbol{n}^s \otimes \boldsymbol{m}^s) \tag{E8b}$$

$$\tau^s_{\mathrm{n}+1} = \boldsymbol{\sigma}_{\mathrm{n}+1} : (\boldsymbol{m}^s \otimes \boldsymbol{n}^s) \tag{E8c}$$

$$\Delta\gamma^s_{n+1} = \left(\frac{\langle|\tau^s_{n+1} - x^s_{n+1}| - r^s_{n+1}\rangle}{k}\right)^m sign(\tau^s_{n+1} - x^s_{n+1})\Delta t_{n+1} \tag{E8d}$$

$$\Delta x^s_{n+1} = A\Delta y^s_{n+1}\;\Delta y^s_{n+1} = \Delta\gamma^s_{n+1} - Dy^s_{n+1}|\Delta\gamma^s_{n+1}| \tag{E8e}$$

$$\Delta r^s_{n+1} = \sum_{t=1}^{N} QH^{st}\Delta q^t_{n+1}\;\Delta q^t_{n+1} = \left(1 - Bq^t_{n+1}\right)|\Delta\gamma^t_{n+1}| \tag{E8f}$$

Differentiating all items in Eq. (E8e), it yields

$$\begin{aligned} \mathrm{d}\Delta x^s_{n+1} &= A\mathrm{d}\Delta y^s_{n+1} \\ &= A\mathrm{d}\Delta\gamma^s_{n+1} - A\mathrm{d}\left(Dy^s_{n+1}|\Delta\gamma^s_{n+1}|\right) \\ &= \frac{1}{1+AD|\Delta\gamma^s_{n+1}|}\left[A - Dx^s_{n+1}\cdot sign(\Delta\gamma^s_{n+1})\right]\mathrm{d}\Delta\gamma^s_{n+1} \\ &= \frac{1}{1+AD|\Delta\gamma^s_{n+1}|}\left[A - Dx^s_{n+1}\cdot sign(\Delta\gamma^s_{n+1})\right]\delta^{st}\mathrm{d}\Delta\gamma^t_{n+1} \end{aligned} \tag{E9}$$

Where $\delta^{st} = 1$ if $s = t$; otherwise, $\delta^{st} = 0$.

Here, a second-ordered tensor $\boldsymbol{L}_1$ is defined, and its components can be given as

$$L^{st}_1 = \frac{1}{1 + AD|\Delta\gamma^s_{n+1}|}\left[A - Dx^s_{n+1}\cdot sign(\Delta\gamma^s_{n+1})\right]\delta^{st} \tag{E10}$$

Then, Eq. (E10) can be rewritten as

$$\mathrm{d}\Delta x^s_{n+1} = L^{st}_1\mathrm{d}\Delta\gamma^t_{n+1} \tag{E11}$$

Differentiating all items in Eq. (E8f), it yields

$$\begin{aligned} \mathrm{d}\Delta r^s_{n+1} &= \sum_{t=1}^{N} QH^{st}\mathrm{d}\Delta q^t_{n+1} \\ &= \sum_{t=1}^{N} QH^{st}\frac{1 - Bq^t_{n+1}}{1 + B|\Delta\gamma^t_{n+1}|}\mathrm{sign}\left(\Delta\gamma^t_{n+1}\right)\mathrm{d}\Delta\gamma^t_{n+1} \end{aligned} \tag{E12}$$

Let $\boldsymbol{L}_2$ be a second-ordered tensor, and its components can be given as

$$L^{st}_2 = QH^{st}\frac{1 - Bq^t_{n+1}}{1 + B|\Delta\gamma^t_{n+1}|}\mathrm{sign}\left(\Delta\gamma^t_{n+1}\right) \tag{E13}$$

Then, Eq. (E12) can be rewritten as

$$\mathrm{d}\Delta r^s_{n+1} = \sum_{t=1}^{N} L^{st}_2\mathrm{d}\Delta\gamma^t_{n+1} \tag{E14}$$

Differentiating all items in Eq. (E8c), it yields

$$\mathrm{d}\tau^s_{n+1} = (\boldsymbol{m}^s \otimes \boldsymbol{n}^s) : \mathrm{d}\boldsymbol{\sigma}_{n+1} \tag{E15}$$

Differentiating all items in Eq. (E8d), it yields

$$\begin{aligned}\mathrm{d}\Delta\gamma^s_{n+1} &= \mathrm{d}\left[\left(\frac{\langle|\tau^s_{n+1}-x^s_{n+1}|-r^s_{n+1}\rangle}{k}\right)^m sign(\tau^s_{n+1}-x^s_{n+1})\Delta t_{n+1}\right] \\ &= \frac{m|\Delta\gamma^s_{n+1}|}{\langle|\tau^s_{n+1}-x^s_{n+1}|-r^s_{n+1}\rangle}\cdot(\mathrm{d}\tau^s_{n+1}-\mathrm{d}\Delta x^s_{n+1}-sign(\tau^s_{n+1}-x^s_{n+1})\mathrm{d}\Delta r^s_{n+1})+\frac{\Delta\gamma^s_{n+1}}{\Delta t_{n+1}}\mathrm{d}\Delta t_{n+1}\end{aligned} \tag{E16}$$

Let us define a second-ordered tensor $\boldsymbol{L}_3$ and a third-ordered one $\boldsymbol{L}_4$ further, and their components can be given, respectively, as

$$L^{st}_3 = \delta^{st} + \frac{m|\Delta\gamma^s_{n+1}|}{\langle|\tau^s_{n+1}-x^s_{n+1}|-r^s_{n+1}\rangle}\cdot(L^{st}_1 + sign(\tau^s_{n+1}-x^s_{n+1})L^{st}_2) \tag{E17a}$$

$$L^{sij}_4 = \frac{m|\Delta\gamma^s_{n+1}|}{\langle|\tau^s_{n+1}-x^s_{n+1}|-r^s_{n+1}\rangle}m^{si}n^{sj} \tag{E17b}$$

Then, combining Eqs. (E11), (E13), (E16) and (E17), it yields

$$\mathrm{d}\Delta\gamma^s_{n+1} = \sum_{t=1}^{N} L^{st}_5 : \left(\boldsymbol{L}^t_4 : \mathrm{d}\boldsymbol{\sigma}_{n+1} + \frac{\Delta\gamma^t_{n+1}}{\Delta t_{n+1}}\mathrm{d}\Delta t_{n+1}\right) \tag{E18}$$

where $\boldsymbol{L}_5$ is the inverse of $\boldsymbol{L}_3$, and $(\boldsymbol{L}^t_4)^{ij} = L^{tij}_4$.

Differentiating all items in Eq. (E8b), it yields

$$\begin{aligned}\mathrm{d}\Delta\boldsymbol{\varepsilon}^{vp}_{n+1} &= \sum_{s=1}^{N}\tfrac{1}{2}(\boldsymbol{m}^s\otimes\boldsymbol{n}^s+\boldsymbol{n}^s\otimes\boldsymbol{m}^s)\mathrm{d}\Delta\gamma^s_{n+1} \\ &= \sum_{s=1}^{N}\tfrac{1}{2}(\boldsymbol{m}^s\otimes\boldsymbol{n}^s+\boldsymbol{n}^s\otimes\boldsymbol{m}^s)\sum_{t=1}^{N}L^{st}_5 : \left(\boldsymbol{L}^t_4 : \mathrm{d}\boldsymbol{\sigma}_{n+1} + \frac{\Delta\gamma^t_{n+1}}{\Delta t_{n+1}}\mathrm{d}\Delta t_{n+1}\right)\end{aligned} \tag{E19}$$

Differentiating all items in Eq. (E8a), it yields

$$\begin{aligned}\mathrm{d}\Delta\boldsymbol{\sigma}_{n+1} &= \boldsymbol{C} : (\mathrm{d}\Delta\boldsymbol{\varepsilon}_{n+1} - \mathrm{d}\Delta\boldsymbol{\varepsilon}^{p}_{n+1}) \\ &= \boldsymbol{C} : \left(\mathrm{d}\Delta\boldsymbol{\varepsilon}_{n+1} - \sum_{s=1}^{N}\tfrac{1}{2}(\boldsymbol{m}^s\otimes\boldsymbol{n}^s+\boldsymbol{n}^s\otimes\boldsymbol{m}^s)\sum_{t=1}^{N}L^{st}_5 : \left(\boldsymbol{L}^t_4 : \mathrm{d}\boldsymbol{\sigma}_{n+1} + \frac{\Delta\gamma^t_{n+1}}{\Delta t_{n+1}}\mathrm{d}\Delta t_{n+1}\right)\right) \\ &= \boldsymbol{C} : \left(\mathrm{d}\Delta\boldsymbol{\varepsilon}_{n+1} - \sum_{s=1}^{N}\tfrac{1}{2}(\boldsymbol{m}^s\otimes\boldsymbol{n}^s+\boldsymbol{n}^s\otimes\boldsymbol{m}^s)\sum_{t=1}^{N}L^{st}_5 : \left(\boldsymbol{L}^t_4 : \mathrm{d}\Delta\boldsymbol{\sigma}_{n+1} + \frac{\Delta\gamma^t_{n+1}}{\Delta t_{n+1}}\mathrm{d}\Delta t_{n+1}\right)\right)\end{aligned} \tag{E20}$$

Let

$$\boldsymbol{H}_1 = \boldsymbol{I} + \boldsymbol{C} : \sum_{s=1}^{N}\frac{1}{2}(\boldsymbol{m}^s\otimes\boldsymbol{n}^s+\boldsymbol{n}^s\otimes\boldsymbol{m}^s)\sum_{t=1}^{N}L^{st}_5 : \boldsymbol{L}^t_4 \tag{E21}$$

Then, Eq. (E20) can be rewritten as

$$\begin{aligned}\mathrm{d}\Delta\boldsymbol{\sigma}_{n+1} &= \boldsymbol{H}_1^{-1} : \boldsymbol{C} \\ &: \left(\mathrm{d}\Delta\boldsymbol{\varepsilon}_{n+1} - \sum_{s=1}^{N}\frac{1}{2}(\boldsymbol{m}^s\otimes\boldsymbol{n}^s+\boldsymbol{n}^s\otimes\boldsymbol{m}^s)\sum_{t=1}^{N}L^{st}_5\frac{\Delta\gamma^t_{n+1}}{\Delta t_{n+1}}\mathrm{d}\Delta t_{n+1}\right)\end{aligned} \tag{E22}$$

Thus, we can obtain that

$$\frac{\mathrm{d}\Delta\boldsymbol{\sigma}_{n+1}}{\mathrm{d}\Delta\boldsymbol{\varepsilon}_{n+1}} = \boldsymbol{H}_1^{-1} : \boldsymbol{C} \tag{E23}$$

$$\frac{\mathrm{d}\Delta\boldsymbol{\sigma}_{n+1}}{\mathrm{d}\Delta t_{n+1}} = -\boldsymbol{H}_1^{-1} : \boldsymbol{C} : \sum_{s=1}^{N}\frac{1}{2}(\boldsymbol{m}^s\otimes\boldsymbol{n}^s+\boldsymbol{n}^s\otimes\boldsymbol{m}^s)\sum_{t=1}^{N}L^{st}_5\frac{\Delta\gamma^t_{n+1}}{\Delta t_{n+1}} \tag{E24}$$

If substitute Eqs. (E23) and (E24) into Eq. (11), the incremental secant modulus tensor is easy to be obtained.

References

[1] Trofimov A, Abaimov S, Sevostianov I. Inverse homogenization problem: Evaluation of elastic and electrical (thermal) properties of composite constituents. Int J Eng Sci 2018;129:34–46.

[2] Ma H, Hu G, Wei Y, Liang L. Inclusion problem in second gradient elasticity. Int J Eng Sci 2018;132:60–78.

[3] Chao X, Qi L, Cheng J, Tian W, Zhang S, Li H. Numerical evaluation of the effect of pores on effective elastic properties of carbon/carbon composites. Compos Struct 2018;196:108–16.

[4] Nguyen V-D, Wu L, Noels L. A micro-mechanical model of reinforced polymer failure with length scale effects and predictive capabilities. Validation on carbon fiber reinforced high-crosslinked RTM6 epoxy resin. Mech Mater 2019;133:193–213.

[5] Tian W, Qi L, Zhou J, Liang J, Ma Y. Representative volume element for composites reinforced by spatially randomly distributed discontinuous fibers and its application. Compos Struct 2015;131:366–73.

[6] Eshelby JD. The determination of the elastic field of an ellipsoidal inclusion, and related problems. Proc Royal Soc London 1957;241:376–96.

[7] Mori T, Tanaka K. Average stress in matrix and average elastic energy of materials with misfitting inclusions. Acta Metall 1973;21(5):571–4.

[8] Kroner E. Berechnung der elastischen Konstanten des Vielkristalls aus den Konstanten des Einkristalls. Zeitschrift für Physik 1958;151(4):504–18.

[9] Budiansky B. On the elastic moduli of some heterogeneous materials. J Mech Phys Solids 1965;13(4):223–7.

[10] Christensen RM, Lo KH. Solutions for effective shear properties in three phase sphere and cylinder models. J Mech Phys Solids 1979;27(4):315–30.

[11] Weng GJ. Some elastic properties of reinforced solids, with special reference to isotropic ones containing spherical inclusions. Int J Eng Sci 1984;22(7):845–56.

[12] Hori M, Nemat-Nasser S. Double-inclusion model and overall moduli of multi-phase composites. Mech Mater 1993;14(3):189–206.

[13] Huang Y, Hu KX, Wei X, Chandra A. A generalized self-consistent mechanics method for composite materials with multiphase inclusions. J Mech Phys Solids 1994;42(3):491–504.

[14] Hill R. A self-consistent mechanics of composite materials. J Mech Phys Solids 1965;13(4):213–22.

[15] Berbenni S, Dinzart F, Sabar H. A new internal variables homogenization scheme for linear viscoelastic materials based on an exact Eshelby interaction law. Mech Mater 2015;81:110–24.

[16] Lavergne F, Sab K, Sanahuja J, Bornert M, Toulemonde C. Homogenization schemes for aging linear viscoelastic matrix-inclusion composite materials with elongated inclusions. Int J Solids Struct 2016;80:545–60.

[17] Barral M, Chatzigeorgiou G, Meraghni F, Léon R. Homogenization using modified Mori-Tanaka and TFA framework for elastoplastic-viscoelastic-viscoplastic composites: Theory and numerical validation. Int J Plast 2020;127:102632. https://doi.org/10.1016/j.ijplas.2019.11.011.

[18] Abaimov SG, Trofimov A, Sergeichev IV, Akhatov IS. Multi-step homogenization in the Mori-Tanaka-Benveniste theory. Compos Struct 2019;223:110801. https://doi.org/10.1016/j.compstruct.2019.03.073.

[19] Tian W, Qi L, Chao X, Liang J, Fu MW. A new interpolative homogenization model for evaluation of the effective elasto-plastic responses of two-phase composites. Compos Struct 2019;210:810–21.

[20] Sun W, Duan C, Yin W. Development of a dynamic constitutive model with particle damage andthermal softening for Al/SiCp composites. Compos Struct 2020;236:111856. https://doi.org/10.1016/j.compstruct.2020.111856.

[21] Yun GJ, Zhu F-Y, Lim HJ, Choi H. A damage plasticity constitutive model for wavy CNT nanocomposites byincremental Mori-Tanaka approach. Compos Struct 2021;258:113178. https://doi.org/10.1016/j.compstruct.2020.113178.

[22] Guo S, Kang G, Zhang J. Meso-mechanical constitutive model for ratchetting of particle-reinforced metal matrix composites. Int J Plast 2011;27(12):1896–915.

[23] Masson R, Zaoui A. Self-consistent estimates for the rate-dependent elastoplastic behaviour of polycrystalline materials. J Mech Phys Solids 1999;47(7):1543–68.

[24] Pierard O, Doghri I. An enhanced affine formulation and the corresponding numerical algorithms for the mean-field homogenization of elasto-viscoplastic composites. Int J Plast 2006;22(1):131–57.

[25] Mercier S, Molinari A. Homogenization of elastic–viscoplastic heterogeneous materials: Self-consistent and Mori-Tanaka schemes. Int J Plast 2009;25(6):1024–48.

[26] Mercier S, Molinari A, Berbenni S, Berveiller M. Comparison of different homogenization approaches for elastic–viscoplastic materials. Modell Simul Mater Sci Eng 2012;20(2):024004. https://doi.org/10.1088/0965-0393/20/2/024004.

[27] Molinari A, Ahzi S, Kouddane R. On the self-consistent modeling of elastic-plastic behavior of polycrystals. Mech Mater 1997;26(1):43–62.

[28] Turner PA, Tomé CN. Self-consistent modeling of visco-elastic polycrystals: application to irradiation creep and growth. J Mech Phys Solids 1993;41(7):1191–211.

[29] Wang H, Capolungo L, Clausen B, Tomé CN. A crystal plasticity model based on transition state theory. Int J Plast 2017;93:251–68.

[30] Wang H, Wu PD, Tomé CN, Huang Y. A finite strain elastic–viscoplastic self-consistent model for polycrystalline materials. J Mech Phys Solids 2010;58(4):594–612.

[31] Molinari A, Canova GR, Ahzi S. A self consistent approach of the large deformation polycrystal viscoplasticity. Acta Metall 1987;35(12):2983–94.

[32] Doghri I, Adam L, Bilger N. MFH of elasto-viscoplastic composites based on a general incrementally affine linearization method. Int J Plast 2010;26:219–38.

[33] Miled B, Doghri I, Brassart L, Delannay L. Micromechanical modeling of coupled viscoelastic–viscoplastic composites based on an incrementally affine formulation. Int J Solids Struct 2013;50(10):1755–69.

[34] Yu C, Kang G, Xie Xi, Rao W. A micromechanical model for the grain size dependent super-elasticity degeneration of NiTi shape memory alloys. Mech Mater 2018;125:35–51.

[35] Brassart L, Stainier L, Doghri I, Delannay L. Homogenization of elasto-(visco) plastic composites based on an incremental variational principle. Int J Plast 2012;36:86–112.

[36] Lahellec N, Suquet P. Effective response and field statistics in elasto-plastic and elasto-viscoplastic composites under radial and non-radial loadings. Int J Plast 2013;42:1–30.
[37] Agoras M, Ponte Castañeda P. Iterated linear comparison bounds for vis-coplastic porous materials with ellipsoidal microstructures. J Mech Phys Solids 2013;61 (3):701–25.
[38] Boudet J, Auslender F, Bornert M, Lapusta Y. An incremental variational formulation for the prediction of the effective work-hardening behavior and field statistics of elasto-(visco) plastic composites. Int J Solids Struct 2016;83:90–113.
[39] Idiart MI, Lahellec N. Estimates for the overall linear properties of pointwise heterogeneous solids with application to elasto-viscoplasticity. J Mech Phys Solids 2016;97:317–32.
[40] Wu L, Adam L, Doghri I, Noels L. An incremental-secant mean-field homogenization method with second statistical moments for elasto-visco-plastic composite materials. Mech Mater 2017;114:180–200.
[41] Rao W, Zhang J, Jiang H, Kang G. Meso-mechanical constitutive model of bulk metallic glass matrix composites. Mech Mater 2016;103:68–77.
[42] Rao W, Zhang J, Kang G, Yu C, Jiang H. A meso-mechanical constitutive model of bulk metallic glass composites considering the local failure of matrix. Int J Plast 2019;115:238–67.
[43] Mura T. Micromechanics of defects in solids. Kluwer Academic Publishers; 1987.
[44] Pierard O, LLorca J, Segurado J, Doghri I. Micromechanics of particle-reinforced elasto-viscoplastic composites: finite element simulations versus affine homogenization. Int J Plast 2007;23(6):1041–60.
[45] Abaqus. Abaqus/Standard User's Manual version 6. 2014.
[46] Li S, Wang G, Sauer RA. The Eshelby tensors in a finite spherical domain-Part II: applications to homogenization. J Appl Mech 2007;74:784–97.
[47] Czarnota C, Kowalczyk-Gajewska K, Salahouelhadj A, Martiny M, Mercier S. Modeling of the cyclic behavior of elastic-viscoplastic composites by the additive tangent Mori-Tanaka approach and validation by finite element calculations. Int J Solids Struct 2015;56-57:96–117.
[48] Robert C, Mareau C. A comparison between different numerical methods for the modeling of polycrystalline materials with an elastic-viscoplastic behavior. Comput Mater Sci 2015;103:134–44.
[49] Peng X, Tang S, Hu N, Han J. Determination of the Eshelby tensor in mean-field schemes for evaluation of mechanical properties of elastoplastic composites. Int J Plast 2016;76:147–65.
[50] Lebensohn RA, Tomé CN. A self-consistent anisotropic approach for the simulation of plastic deformation and texture development of polycrystals: Application to zirconium alloys. Acta Metall Mater 1993;41(9):2611–24.